Diffusion weighted imaging in the normal appearing white matter of glioma patients

PhD Thesis

Andrea Horváth, MD

Supervisors:

Prof. Péter Bogner, MD, PhD

Prof. Tamás Dóczi, MD, DSc

Program Director: Prof. András Büki, MD, DSc

Doctoral School Director: Prof. Sámuel Komoly, MD, DSc

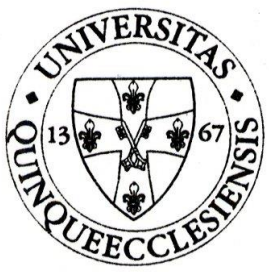

University of Pécs, Medical School

Clinical Neuroscience Doctoral School

Pécs, 2016

Table of contents

List of abbreviations

3D	three dimensional
ADC	apparent diffusion coefficient
ADC_{fast}	apparent diffusion coefficient of the fast diffusion component
ADC_{slow}	apparent diffusion coefficient of the slow diffusion component
ANOVA	analysis of variance
CHARMED	composite hindered and restricted model of diffusion
CNS	central nervous system
CSF	cerebrospinal fluid
DICOM	digital imaging and communications in medicine
DTI	diffusion tensor imaging
DWI	diffusion weighted imaging
EPI	echo planar imaging
FLAIR	fluid attenuated inversion recovery
FLIRT	Oxford Centre for Functional MRI of the Brain (FMRIB)'s linear image registration tool
FOV	field of view
FMRIB	Oxford Centre for Functional MRI of the Brain, Oxford, UK
FSL	FMRIB's software library
GRAPPA	generalized autocalibration partially parallel acquisition
IDH	isocitrate dehydrogenase
IL-6	interleukin- 6
MGH	Massachusetts General Hospital, Boston, MA
MGMT	O6-methylguanine-DNA methyltransferase
MPRAGE	magnetization prepared rapid gradient-echo

MR	magnetic resonance
MRI	magnetic resonance imaging
NAWM	normal appearing white matter
PWI	perfusion weighted imaging
ROI	region of interest
TE	echo time
TI	inversion time
TR	repetition time
VEGF	vascular endothelial growth factor
WHO	world health organization
WM	white matter

1. Introduction

Central nervous system (CNS) neoplasms affect adults and children of all ages, and they are the second leading-cause of tumor-related death in children and adolescents (Ostrom et al., 2015). CNS tumors are classified as primary tumors, if they arise from brain tissue cells, or metastatic tumors, if they originate from cancers outside of the CNS. Glial cell-derived tumors account for 27% of all primary CNS tumors, and 80% of malignant CNS neoplasms. The annual incidence is 18 054 /100 000 individuals and they occur at a rate of 5.55/100 000 individuals annually in the United States according to the Central Brain Tumor Registry of the United States (Ostrom et al., 2015). They require special attention in the field of neurooncology due to their complex behavior and histopathology and relatively high mortality rate.

Many advanced neuroimaging methods have been developed during the past decades that provide not only structural but functional information on the behavior of gliomas. These techniques, including diffusion weighted imaging (DWI), MR spectroscopy, and perfusion weighted MR imaging (PWI) allow us to aid appropriate treatment planning, detect early treatment response and evaluate prognosis (Puttick et al., Law et al., 2003, Cha, 2006, Larsen et al., 2013, Roy et al., 2013). They are currently being validated and increasingly incorporated into daily clinical practice (Essig et al., 2012, Essig et al., 2013).

Despite the improvements of diagnostic methods and surgical techniques and the intense effort in developing new, targeted therapies (Olson et al., 2014) the prognosis for patients with glioma still remains poor (Tsai et al., 2003, Yoshiura et al., 2010). Only 5.1% of patients with the most malignant glioma subtype survive 5 years after diagnosis (Stupp and Roila, 2009, Ma et al., 2014, Ostrom et al., 2015). A possible reason for the poor prognosis is the diffuse, infiltrative nature of gliomas which hinders complete resection and reduces the efficacy of local radiation therapy or radiosurgery (Giese et al., 2003).

Tumor infiltration in macroscopically inconspicuous areas distant from the tumor was shown by Sahm et al. in post mortem human brains (Sahm et al., 2012). Recently, several research groups tried to show tumor infiltration with magnetic resonance imaging. In particular, Ingelese et al., Maudsley et al. and Kallenberg et al. revealed abnormalities in the contralateral normal appearing white matter (NAWM) of glioma patients with diffusion tensor imaging (DTI) and whole brain

spectroscopy (Cohen et al., 2005, Inglese et al., 2006, Maudsley et al., 2013, Kallenberg et al., 2014), and they explained their findings with the presence of tumor infiltration. However, the question may arise, whether these diffusion alterations are really related to infiltrative tumor cells, and whether apparent diffusion coefficient (ADC) can be used as a marker of tumor infiltration. In order to develop efficient therapies and to make appropriate treatment decisions, it is necessary to know as much as it is possible about the behavior of gliomas.

1.1 Glioma grading

Glioma grade is assessed according to the 2007 Word Health Organization (WHO) classification and it reflects tumor malignancy, taking into account mitotic activity, cellularity, nuclear atypia, pleomorphism, endothelial proliferation and necrosis (Louis et al., 2007). WHO classification subdivides gliomas into four grades (I-IV) and provides the basis for assessing prognosis and guiding therapy. However, histologically identical gliomas might have different clinical outcome and treatment response. To overcome this limitation, molecular markers such as isocytrate dehydrogenase (IDH) mutation, 1p19q codeletion and methylguanine-methyltransferase (MGMT) promoter methylation status are recently being incorporated in the diagnosis (Louis et al., 2014, Siegal, 2015).

Tumor grading is based on biopsy samples. However the sampling error rate is high due to the great heterogenity inside the tumor. MR imaging has an important role in revealing the most malignant part of gliomas and determining the accurate site for biopsy (Cha, 2006).

1.2 Glioma behavior

Gliomas exhibit a high recurrence rate which is possibly related to their infiltrative ability and remarkable neoangiogenesis (Mikkelsen et al., 1995). Glioma recurrence after surgery usually occurs adjacent to the resection cavity (Bashir et al., 1988). Gliomas can disseminate great distances from the original tumor. Infiltration takes place along white matter tracts, along blood vessels and beneath the pia mater. However, the invasiveness does not depend on tumor grade, low grade gliomas often exhibit extensive infiltration (Giese et al., 2003). It has been shown, that migrating glioma cells have reduced proliferation rate and a relative resistance to apoptosis which might explain their resistance to

chemoradiation (Giese et al., 1996). The invasive cells can regain their proliferative ability and establish a recurrent tumor (Giese et al., 2003). Regrowth of a recurrent tumor depends on neovascularization (Folkman, 1990) in which vascular endothelial growth factor (VEGF) plays a critical role (Plate et al., 1992).

1.3 Magnetic resonance imaging of gliomas

1.3.1 Morphological MR imaging of gliomas

MR imaging plays an important role in the diagnosis and treatment planning of CNS neoplasms. Conventional MR imaging provides information about tumor location, tumor morphology, extent and its relationship to surrounding structures. It allows differential diagnosis between tumoral and pseudotumoral lesions in more than 50% of cases. The standard protocol includes T2-weighted imaging, unenhanced T1-weighted scans, fluid attenuated inversion recovery (FLAIR) sequence and post-contrast T1-weighted imaging (Essig et al., 2012) (Fig. 1).

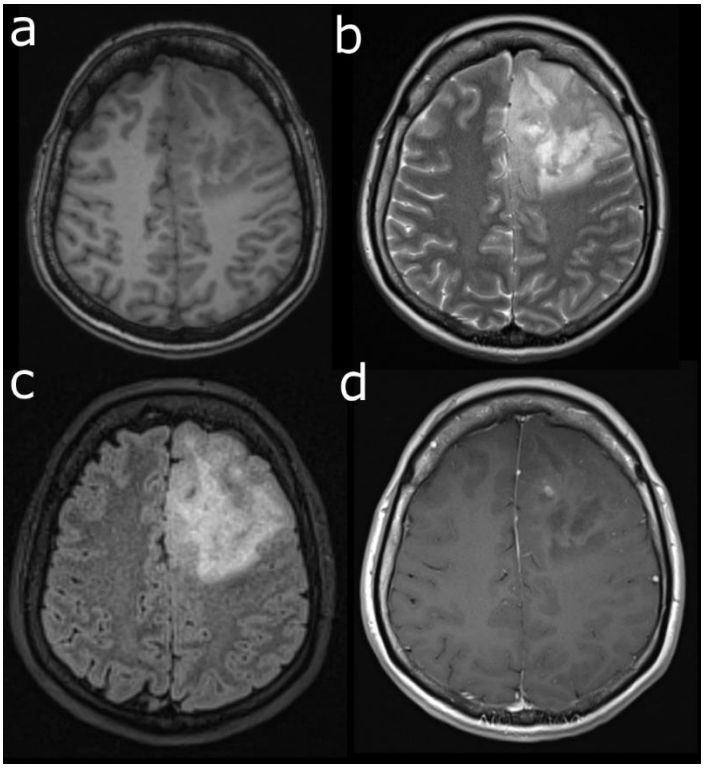

Fig. 1. a) Nonenhanced T1 weighted MPRAGE, b) T2 weighted c) FLAIR, d) post-contrast T1-weighted spin echo sequence of a patient with grade II oligodendroglioma. Images were acquired at the Diagnostic Centre of Pécs.

Gliomas might appear heterogeneous on conventional scans due to the presence of necrosis, hemorrhage or calcification. In general, gliomas appear hypointense on unenhanced T1-weighted scans due to their prolonged T1 relaxation time. On T2-weighted scans they are hyperintense because of their prolonged T2 relaxation time. FLAIR images enable better distinction of tumor and edema (Essig et al., 2001).

Contrast enhanced scans with gadolinium-based contrast media improve brain tumor visualization, since gadolinium chelates pass through the disrupted blood brain barrier and accumulate in the tumor tissue. Contrast enhancement increases the sensitivity and specificity of MR examinations (Runge et al., 1992).

1.3.2 Physiological MR imaging of gliomas

Besides anatomical images, physiological information on brain tumor behavior is now also available. Advanced neuroimaging enables to characterize functional, metabolic, cellular, hemodynamic and cytoarchitectal alterations. Diffusion weighted imaging aids the assessment of tumor cellularity while diffusion tensor imaging (DTI) tractography is used to avoid injuring important white matter tracts during surgery. Tumor malignancy can be determined with perfusion weighted imaging (PWI) by measuring the degree of angiogenesis and capillary permeability. Therefore PWI can be used for biopsy guidance, for the assessment of tumor grade and prognosis, for monitoring treatment response and for differentiation of recurrence from radiation necrosis. MR spectroscopy provides noninvasive metabolic information on brain tumors (Cha, 2006).

1.4 Diffusion weighted imaging

1.4.1 Technical aspects of diffusion weighted imaging

1.4.1.1 Physical basis of diffusion weighted imaging

Molecular diffusion is a thermal energy-driven random molecular motion called Brownian motion. Mean square displacement during free diffusion is proportional with the diffusion coefficient, the diffusion time and is statistically described by Einstein equation,

$$R^2 = 2 \cdot D \cdot t \quad (1)$$

where R^2 is the mean square displacement, D is the diffusion coefficient and t is the diffusion time.

1.4.1.2 Diffusion encoding

Diffusion can be measured with diffusion-sensitive sequences by using diffusion encoding gradients. Diffusion sensitivity of a sequence depends on the amplitude of the diffusion gradient (G), the gradient duration (δ), the temporal separation of gradients (Δ) and can be determined by the b factor:

$$b = \gamma^2 \cdot \delta^2 \cdot G^2 \cdot \left(\Delta - \frac{1}{3}\delta\right), \quad (2)$$

where γ is the gyromagnetic ratio.

The most widely used diffusion sensitive sequence is the Stejskal-Tanner pulsed gradient spin-echo sequence which is shown schematically on Fig. 2. In this sequence, two identical, matched diffusion-encoding gradient pulses are applied before and after the 180° refocusing radio frequency pulse (Stejskal and Tanner, 1965).

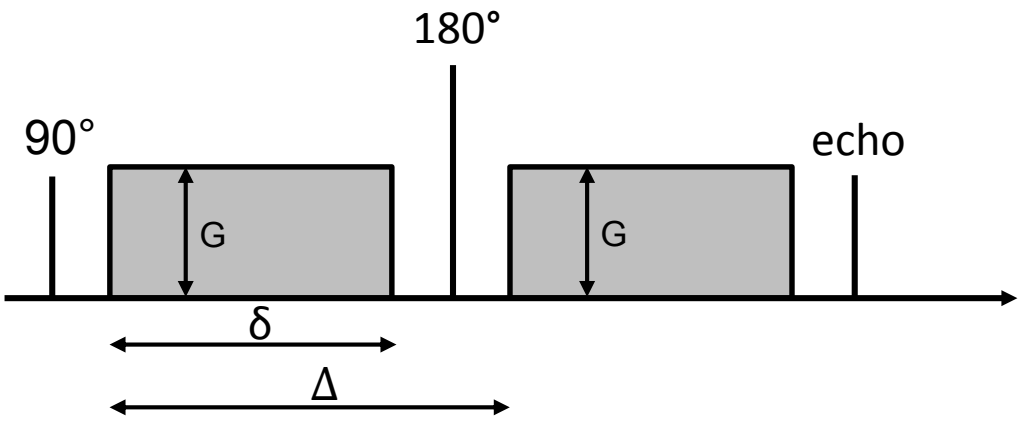

Fig. 2. The Stejskal-Tanner sequence. The diffusion-encoding gradients are applied in two matched pulses. G: gradient amplitude, δ: gradient duration, Δ: temporal separation of gradients.

During the first diffusion-encoding gradient the spins accumulate a phase shift. If the spins are static, this phase shift is cancelled out by the second gradient since that has an identical magnitude as the first one, but opposite sign due to the 180°pulse. For the spins that have changed position due to diffusion, the phase shifts are different resulting in signal loss.

1.4.1.3 Diffusion quantification and ADC

If water molecule displacement is assumed to be Gaussian, there is a single exponential relationship between the MR signal and the ADC, and the coupling factor is the b-factor. The degree of MR signal attenuation can be expressed with the following formula:

$$\frac{S}{S_0} = e^{b \cdot ADC} \quad (3)$$

where S_0 is the signal intensity in the absence of diffusion weighting and S is the signal intensity in the presence of diffusion weighting (Stejskal and Tanner, 1965) (Fig. 3).

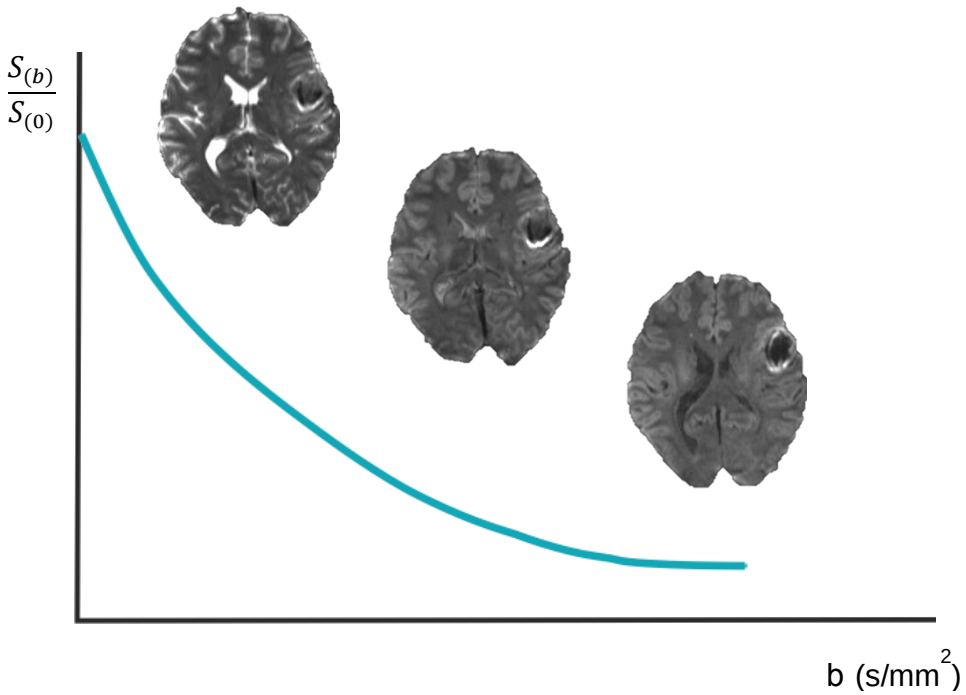

Fig. 3. Signal decay curve as a function of b value. The set of diffusion-weighted images is acquired with different b values. Overall signal intensity in each voxel decreases with the b-value. Tissues with fast diffusion, such as ventricles become hypointense more rapidly with the increase of b value than tissues with slow diffusion.

In order to quantify diffusion, signal intensity needs to be measured with multiple, but at least two b factors. In a clinical setting, typically two b factors, 0 and 1000 are used.

After performing linear fit between $\ln\frac{S_0}{S}$ and b, ADC can be calculated in a region of interest (ROI) or voxel-by voxel as the slope of a linear regression (Le Bihan et al., 1986) (Fig. 4).

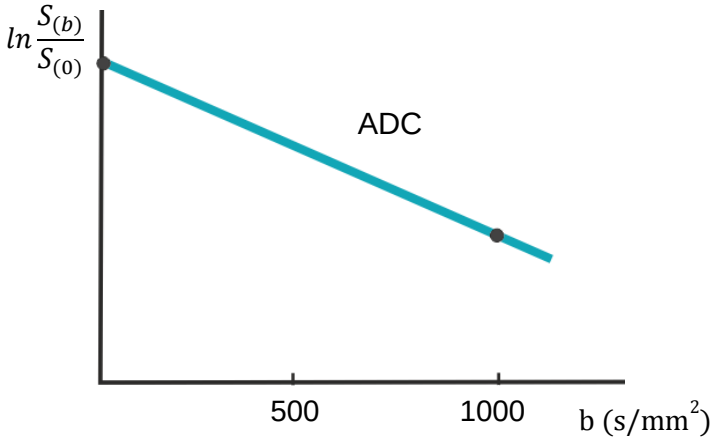

Fig. 4. Monoexponential signal decay curve of water signal in MR. The logarithm of the diffusion MR signal attenuation curve ($\ln\frac{S_{(b)}}{S_{(0)}}$) is shown against the b value. The slope of the curve represents the ADC value.

Voxel-by voxel calculation of ADC values results in an ADC map. In the ROI approach curve fitting is performed on mean signal intensity values from a ROI.

1.4.1.4 Diffusion weighted imaging with extended b value range

Water diffusion in the brain is not a free random walk process, and it cannot be modeled accurately by Gaussian distribution. Free water movement is affected by tortuosity in the extracellular space (Chen and Nicholson, 2000) and by macromolecular crowding and high viscosity in the intracellular space (Hazlewood et al., 1991) (Fig. 5).

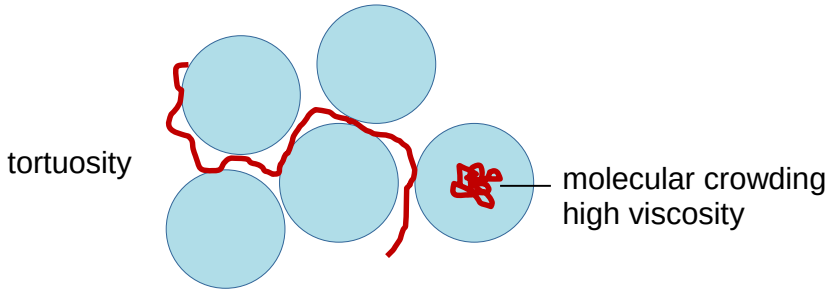

Fig. 5. Schematic illustration of factors that affect free water motion in the brain. In the intracellular space, water movement is affected by macromolecular crowding and high viscosity, while in the intracellular space it is influenced by tortuosity.

Three major modes of diffusion are present in the brain: free, hindered and restricted diffusion (Le Bihan, 1995). Clear restriction diffusion behavior of water has not been measured in vivo yet. Longer diffusion times and diffusion weighting is required to distinguish restricted diffusion from hindered diffusion (Le Bihan and Johansen-Berg, 2012).

With increasing diffusion sensitization (i.e. by increasing the b factor), signal decay deviates from monoexponential (Assaf and Cohen, 1998b, Sugahara et al., 1999, Le Bihan, 2007). The relationship of this non-monoexponential signal decay to morphological or physiological components is yet unclear.

Parametric and non-parametric approaches have been developed to analyze the non-monoexponential signal decay. The parametric approach uses a mathematical model to describe signal decay either based on the diffusion or the morphological components of the tissue. The non-parametric approach does not provide compartment specific information, but it measures non-Gaussian diffusion with a higher sensitivity.

1.4.1.4.1 Non-parametric methods

The non-parametric approach includes q-space imaging (Assaf and Cohen, 2000), diffusion spectrum imaging (Wedeen et al., 2005), diffusion kurtosis imaging, which quantifies the deviation from a Gaussian distribution (Jensen et al., 2005, Kiselev and Il'yasov, 2007), the stretched exponential model (Bennett et al., 2003) and the statistical model (Yablonskiy et al., 2003).

Diffusion MRI could be used as a microstructural probe, if certain diffusion processes can be connected to a specific tissue compartment. However, these model-free approaches are rather phenomenological. Although they fit the signal decay well, the relationship of these parameters to actual tissue structure or compartment is not straightforward (Jensen and Helpern, 2010).

1.4.1.4.2 The biexponential diffusion model and other parametric models

The MR signal decay curve as a function of b value is well fitted with a biexponential function. The model assumes a fast and slow diffusion pool with fast and slow diffusion coefficients (Niendorf et al., 1996, Assaf and Cohen, 1998a):

$$\frac{S_{(b)}}{S_{(0)}} = p_{fast}e^{-b\cdot ADC_{fast}} + p_{slow}e^{-b\cdot ADC_{slow}} \quad (4)$$

where S_b is the signal intensity in the presence of diffusion sensitization, S_0 is the signal intensity in the absence of diffusion sensitization, ADC_{fast} and ADC_{slow} are the ADC values, and p_{fast} and p_{slow} are the contributors to the signal of the fast and slow diffusing water compartments (p_{slow} = 1-p_{fast}). Fig. 6. shows the biexponential signal decay curve.

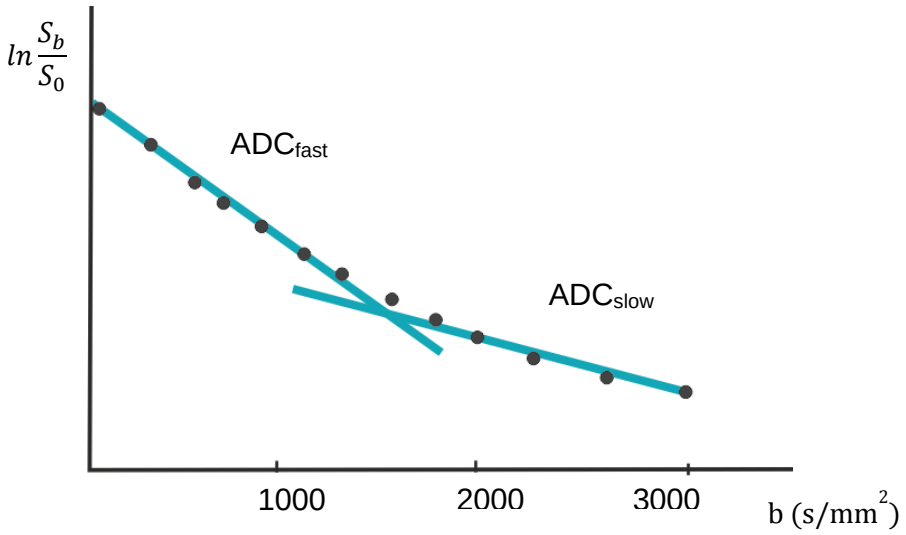

Fig. 6. Biexponential signal decay curve of water signal in MR. Normalized signal attenuation (Sb/S0) on a logarithmic scale as a function of b-value. The slopes of the two lines represent the ADC values of the fast and slow diffusion pool.

At b=0 s/mm^2 most of the signal originates from the fast diffusion component, at b=1000 s/mm^2 the relative signal contribution becomes reversed, while at b=5000 s/mm^2 almost all of the signal comes from the slow diffusion component (Niendorf et al., 1996).

The origin of the slow and fast diffusion pool is yet unclear. It has been thought that the slow diffusion component may represent the intracellular space while the fast diffusion pool might represent the extracellular space. However, the volume fractions of the slow and fast diffusion pools obtained with the biexponential analysis (0.3 and 0.7, respectively) (Niendorf et al., 1996) are approximately the reverse of what is known for the intra- end extracellular water fractions (0.8 and 0.2, respectively) (Nicholson and Sykova, 1998).

A geometric model proposed by Stanisz et al. shows that cylindrical membranes can cause restriction that leads to pseudo-biexponential behavior in nerves. This model describes three diffusion components: diffusion in ellipsoids (representing axons), diffusion in spheres (i.e. glial cells) and diffusion in extracellular matrix (Stanisz et al., 1997). However, this model was specific for optic nerve. The composite hindered and restricted model of diffusion (CHARMED) (Assaf et al., 2004) assumes an intra-axonal water compartment with restricted diffusion and an extra-axonal water compartment with hindered diffusion which can account for pseudo-biexponential behavior. However, this model is not applicable for gray matter.

The most reasonable explanation of the origin of the biexponential signal decay has been proposed by Le Bihan (Le Bihan, 2007). According to his theory, the fast and slow diffusion pool does not originate from a specific compartment, but from two differently structured water pools partly in the extracellular space and partly in the intracellular space. Specifically, the slow diffusion pool corresponds to highly structured water layers bound to membrane surfaces and cytoskeleton by electrostatic forces (i.e. hydration shell around proteins and macromolecules) and the fast diffusion pool originates from the remaining extra and intracellular tissue water (Le Bihan, 2007, Mulkern et al., 2009, Le Bihan and Johansen-Berg, 2012). Fig. 7. illustrates this biphasic water diffusion model.

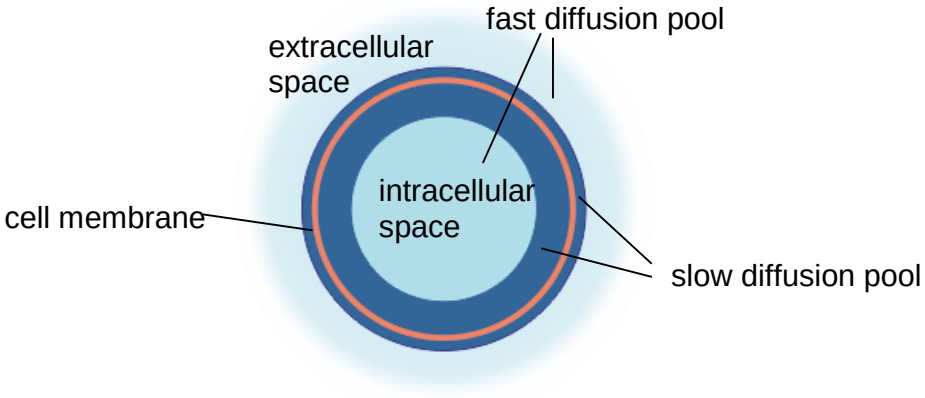

Fig. 7. Biphasic water diffusion model. Slow diffusion pool corresponds to structured water layer attached to protein membranes and cytoskeleton. The remaining extra- and intracellular water contributes to the fast diffusing pool.

In general, diffusion imaging with an extended b factor range enables more specific tissue characterization and differentiation, and can be beneficial in more complete understanding of diseases.

1.4.2 Clinical aspects of diffusion weighted imaging

1.4.2.1 Diffusion imaging in the normal brain: ADC and diffusion contrast

Random motion of tissue water in the brain is affected by cell membranes, cystoskeleton and macromolecules. Therefore DWI provides valuable information about tissue microstructure, and it can be used to monitor changes accompanying various pathologies (Le Bihan, 2007).

Although water displacement is on the order of microns during generally used diffusion times, these microscopic displacement distributions of water molecules within a voxel are integrated to provide a millimetric resolution. Therefore the diffusion coefficient in MRI is called apparent diffusion coefficient and it summarizes all physical processes occurring at a smaller scale at the voxel level (Le Bihan, 2013).

Diffusion weighted imaging provides different contrast compared to relaxation-weighted magnetic resonance imaging. At a given b-factor, areas with high mobility of water molecules such as cerebrospinal fluid appear hyperintense on ADC maps and hypointense on DWI scans. On the other hand, tissues with

slow diffusion (e.g. gray matter) show low signal intensity on ADC maps and high signal intensity on DWI scans (Le Bihan, 2013). Fig. 8. represents the typical diffusion images of a healthy subject.

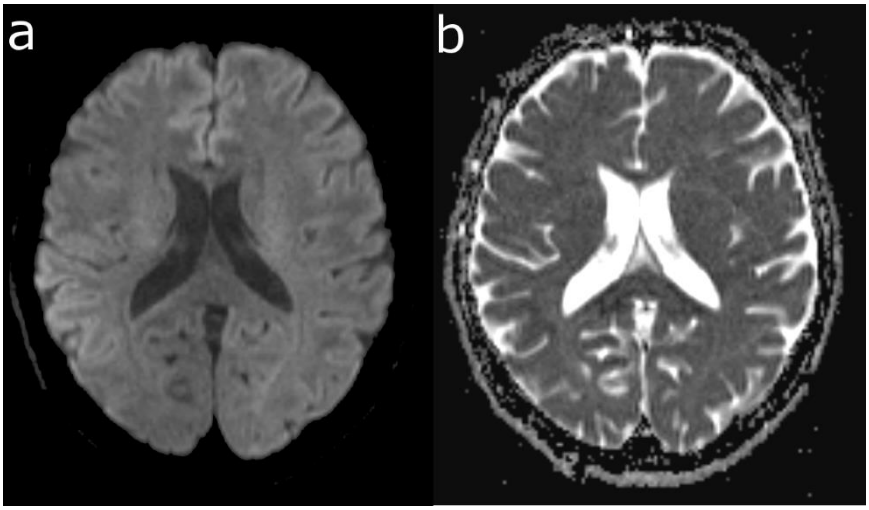

Fig. 8. Diffusion images of a healthy subject. a) DWI image with b=1000 s/mm^2 b) ADC map

In general, ADC in the cerebral cortex is higher than in normal white matter due to its higher water content, and higher blood flow. Mean ADC value of the normal white matter is $7.05\pm0.14\cdot10^{-4}$mm^2/s (Maier et al., 1998) while in the normal deep grey matter it is $7.50\pm0.3\cdot10^{-4}$mm^2/s (Helenius et al., 2002). Mean ADC value measured in the cerebrospinal fluid (CSF) is $30.02\pm1.6\cdot10^{-4}$mm^2/s (Helenius et al., 2002).

Regarding biexponential parameters, ADC_{fast} obtained with biexponential fitting is 50-70% higher than ADC derived from monoexponential fitting. In the normal frontal white matter the mean biexponential parameters are as follows: ADC_{fast} is $11.55\pm0.46\cdot10^{-4}$mm^2/s, ADC_{slow} is $1.25\pm0.14\cdot10^{-4}$mm^2/s while p_{slow} is 30.1±0.50%. In the cortical grey matter, mean ADC_{fast} is $11.42\pm1.06\cdot10^{-4}$mm^2/s, ADC_{slow} is $3.38\pm0.27\cdot10^{-4}$mm^2/s while p_{slow} is 37.8±0.38% (Maier and Mulkern, 2008).

1.4.2.3 Diffusion imaging in pathological conditions

Different pathological conditions imply volume fraction changes of intra- and extracellular spaces because of cell swelling or shrinking which leads to altered ADC value. In acute brain ischemia, cell swelling is associated with cytotoxic edema. This results in more restricted water diffusion which is indicated by a drop of ADC values (Sotak, 2004). Similarly, increased cellularity also leads to lower ADC values. In vasogenic edema, the increased amount of tissue bulk water leads to an increase of mean ADC value (Ebisu et al., 1993). Fig. 9. illustrates how water diffusion is altered in different pathological conditions.

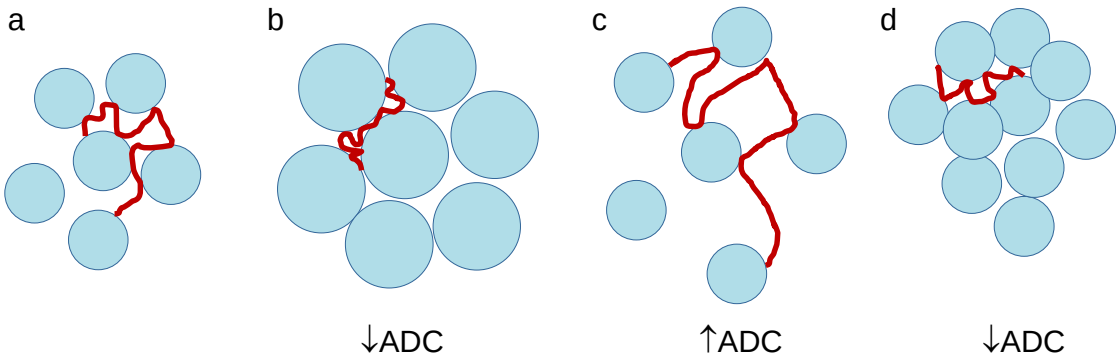

Fig. 9. Schematic illustration of water diffusion in different pathological conditions. a) normal brain b) cytotoxic edema c) vasogenic edema d) cell proliferation

Regarding biexponential diffusion parameters, their pattern can be specific for certain conditions. In cytotoxic edema accompanying acute stroke, the surface area of cell membranes increases due to cell swelling, thus the amount of membrane-bound water rises which results in higher p_{slow} values (Fig. 10). The increase of the slow diffusion compartment implies the reduction of the fast diffusion component that depresses ADC_{mono}, while ADC_{fast} and ADC_{slow} remain relatively unchanged (Le Bihan, 2007, Yoshiura et al., 2010).

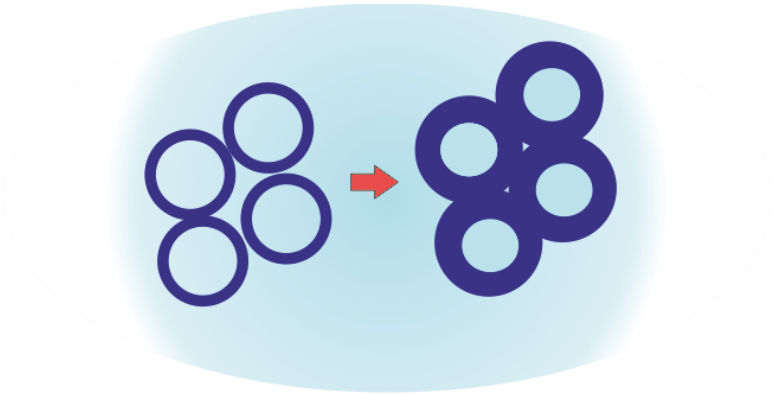

Fig. 10. Changes in water diffusion pool sizes according to the biphasic water model as a result of cell swelling. The amount of membrane-bound water (i.e. the volume fraction of the slow diffusion pool) increases.

On the other hand, in vasogenic edema, ADC_{mono}, ADC_{fast} and ADC_{slow} increase, while p_{slow} decreases because of the greater amount of tissue bulk water (Maier et al., 2001, Maier et al., 2010, Schwarcz et al., 2007).

Table 1. (Maier et al., 2010) summarizes biexponential diffusion parameter changes in different pathologies.

Table 1. Biexponential diffusion parameters in pathological tissues compared to values measured in the normal white matter

	ADC_{mono}	ADC_{fast}	ADC_{slow}	p_{slow}
cytotoxic edema	↓↓	-	-	↑↑
vasogenic edema	↑↑↑	↑	↑	↓↓↓
LGG	↑↑	↑	-	↓↓
HGG	↑	↑	-	↓

Arrows show the relationship of pathological values compared to values measured in normal white matter.

LGG: low grade glioma, HGG: high grade glioma. ADC_{mono}: apparent diffusion coefficient, ADC_{fast}: ADC of the fast diffusion component, ADC_{slow}: ADC of the slow diffusion component, p_{slow}: volume fraction of the slow diffusion component

1.4.2.4 Diffusion imaging of gliomas

1.4.2.4.1 Tumor cellularity and glioma grading

Inverse correlation has been shown between glioma grade and minimum ADC (Bulakbasi et al., 2004, Kitis et al., 2005). High grade tumors are more hypercellular that results in the reduction of extracellular space. This implies the restriction of proton movement that results in decreased ADC (Fig. 9). Diffusion imaging therefore could be used to assess tumor grade (Sugahara et al., 1999). However, there is a significant overlap among ADC values of different tumor grades which prevents using DWI for definitive diagnosis.

It must be noted, that ADC values in gliomas are still higher than ADC values measured in the normal grey or white matter even in the case of high grade gliomas. This might be a result of intratumoral edema due to the compression of microcirculation around the tumor, and to the altered permeability of pathological vessels (Steen, 1992).

The biexponential diffusion analysis shows higher ADC_{mono} and lower p_{slow} values in gliomas compared to normal tissues which might be due to altered blood brain barrier permeability and intratumoral edema (Steen, 1992) or to destruction of extracellular matrix structure by tumor infiltration (Morita et al., 2005). ADC_{mono} declines while p_{slow} rises with the increase of cellularity (i.e. tumor grade), since the amount of membrane-bound water increases (Maier et al., 2001, Le Bihan, 2007, Maier et al., 2010) (Fig. 11).

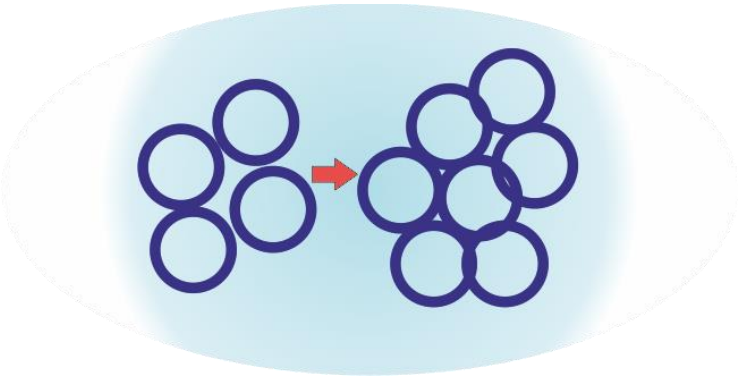

Fig. 11. Changes in water diffusion pool sizes according to the biphasic water model as a result of cell proliferation. The amount of membrane-bound water increases due to the higher amount of cell membranes.

1.4.2.4.2 Response to therapy

Diffusion imaging can predict early tumor response to therapy since decrease in cellularity or radiation- or chemotherapy-induced necrosis is associated with an increase in ADC. Afterwards, ADC returns to baseline value. Sometimes lower ADC values are observed after treatment due to inflammatory cell infiltration, dehydration or disease recurrence (Moffat et al., 2005). An initial decrease of ADC values might occur after anti-angiogenic treatment, since antiangiogenic drugs normalize microvascularization which results in a decrease of edema (Batchelor et al., 2007). In case of unresponsive disease, ADC values remain unchanged. Progressive disease leads to decreasing ADC values due to cell proliferation. If the tumor grows rapidly with necrosis, ADC values can increase which is not related to treatment response in this case (Thoeny et al., 2010). Fig. 12 illustrates how ADC can change in response to treatment.

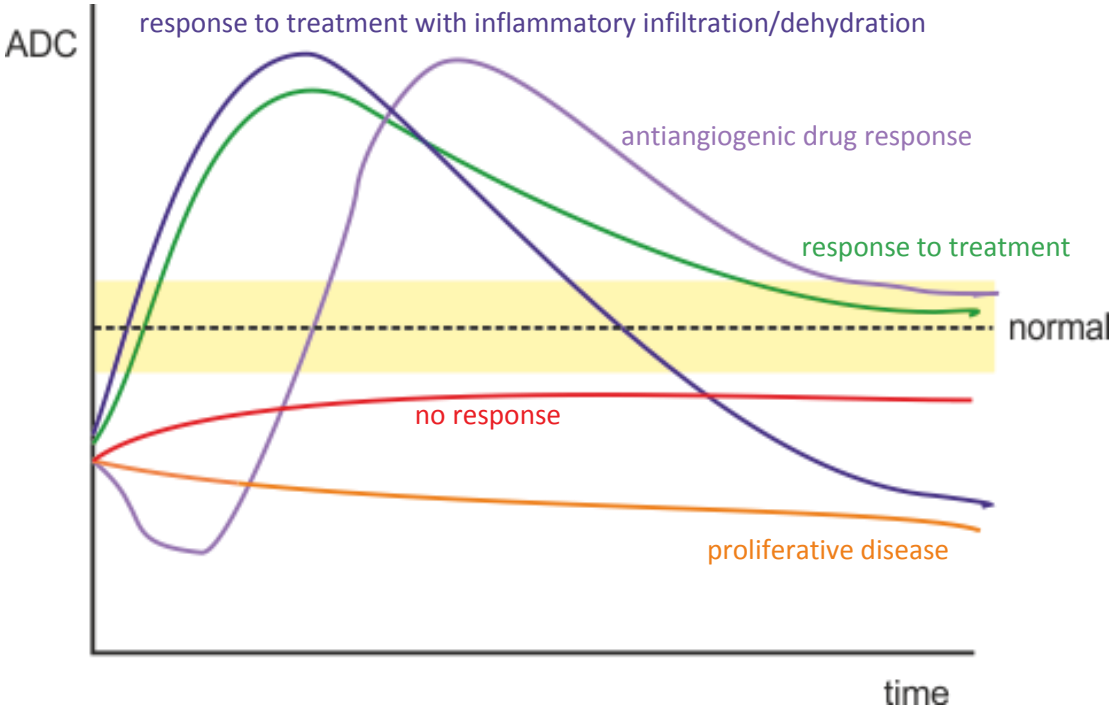

Fig. 12. Changes of ADC values in response to treatment. Broken line represents normal ADC value in the white matter, while the yellow zone indicates the normal ADC value range. Green line: response to treatment, blue line: response to treatment with inflammatory infiltration or dehydration, purple line: antiangiogenic drug response, red line: no response, orange line: proliferative disease.

1.4.2.4.3 Assessing peritumoral edema

Diffusion imaging might support the differential diagnosis of infiltrative and non-infiltrative brain tumors by differentiating vasogenic and infiltrative peritumoral edema. In the peritumoral region of infiltrative tumors lower ADC values are present then in that of non-infiltrative tumors (Lu et al., 2003).

1.4.2.4.4 Integrity of white matter tracts

Gliomas can infiltrate or dislocate white matter tract which can have an impact in surgical planning. DTI can visualize white matter tracts in the surrounding of the tumor which enables accurate planning and evaluation of surgical risks (Wieshmann et al., 2000).

1.4.2.5 Diffusion imaging of normal appearing white matter

The development of diffusion imaging has allowed to measure white matter structure properties in vivo. Although diffusion imaging is a sensitive tool for the detection of subtle changes, diffusion parameters are not specific for a certain tissue characteristic such as fiber density or myelination. The exact relationship between diffusion parameters in the white matter and the underlying tissue structure is still controversial (Rowley et al., 1999). Nevertheless, myelin and cell membranes play a key role in affecting water mobility in the CNS. Besides being sensitive to fiber density, diameter and degree of myelination, diffusion imaging depends on orientation. Therefore, variation in any of these characteristics implies a change in diffusion parameters (Le Bihan, 1995).

There are individual differences in white matter microstructure in healthy subjects which are considered normal (Johansen-Berg, 2009). Besides this, ADC shows a gradual increase with age (Naganawa et al., 2003). There are also slight differences in mean ADC values between white matter regions (Klimas et al., 2013).

The increase of ADC in the NAWM has been previously observed in other diseases. In multiple sclerosis, diffusion abnormality is explained by the loss of myelin sheath (Nagy et al., 2013a, Orsi et al., 2014). In epilepsy, increased ADC in the NAWM correlated with age at onset (Nagy et al., 2016).

In glioma patients increased ADC was found in the NAWM of the unaffected hemisphere. This alteration was explained by the effect of infiltrative tumor cells

(Inglese et al., 2006, Maudsley et al., 2013, Kallenberg et al., 2014) without actually attempting to investigate the effect of tumor infiltration itself or finding other possible explanations.

1.5 Technical aspects of white matter segmentation

White matter can be segmented manually or automatically. Manual segmentation takes long time and requires a trained anatomist or technician. Besides this, structures are distinguished based on signal intensities alone in the manual analysis, which challenging and subjective due to the overlap between class distributions.

Automatic segmentation tools have been developed recently, which take spatial information into account besides many other factors. The most commonly used tools are FMRIB Software Library's (FSL) FMRIB's Automated Segmentation Tool and FreeSurfer's volume based segmentation tool.

1.5.1 FreeSurfer's volume based segmentation tool

FreeSurfer is a program package for analysis and visualization of structural and functional brain image data. Besides many functions, It includes an automatic subcortical segmentation tool, which assigns each voxel in the normalized brain volume to one of approximately forty labels (Fischl et al., 2002), and a surface-based stream that segments the cerebral cortex (Fischl et al., 1999).

White matter can be segmented using the subcortical segmentation stream. After converting images from DICOM to MGH (Massachusetts General Hospital) format and resampling them to coronal $1mm^3$ isotropic voxel-size images, images are registered to MNI305 space (Collins et al., 1994). Then, intensity normalization is performed and non-brain tissues, such as skull, eyes, neck, are removed (Segonne et al., 2004). This is followed by linear volumetric registration to MNI305 atlas and a further intensity normalization. Next, nonlinear volumetric alignment to the MNI305 space is performed. Finally, volumes are labeled based on subject-specific measured values and the Gaussian classifier atlas (GCA) that includes a set of subjects whose structures were manually labeled and then mapped into MNI305 space (Fischl et al., 2002, Fischl et al., 2004). Fig. 13 represents the output of the volumetric segmentation.

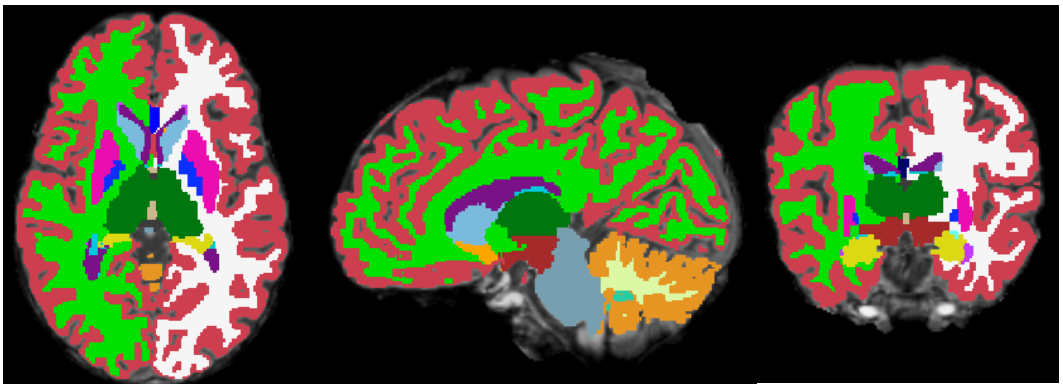

Fig. 13. Output of Freesurfer's volume based segmentation (axial, sagittal and coronal images). White matter of the left hemisphere is marked with white, while white matter of the right hemisphere is labeled with green color. ROIs are placed on MPRAGE scans.

Further parcellation of white matter into regions (i.e. temporal, frontal, parietal and occipital white matter) is possible by using the output from the surface-based (cortical) stream. White matter regions are labeled according to the adjacent cortical area (frontal, temporal, parietal, occipital). Detailed information on FreeSurfer tools and analysis steps can be found at FreeSurferWiki (https://surfer.nmr.mgh.harvard.edu/fswiki).

2. Objectives

The primary aim of this thesis was to clarify the nature of elevated ADC in the NAWM of glioma patients.

An indirect way to prove or exclude the role of distant tumor infiltration in altering diffusion in the contralateral NAWM is to examine the contralateral NAWM of patients with non-infiltrative tumors (e.g. meningiomas). If ADC is elevated in the NAWM of both infiltrative tumor (i.e. glioma) and non-infiltrative tumor (i.e. meningioma) patients, the diffusion alteration cannot be explained exclusively by the presence of tumor infiltration.

Therefore, the primary aim of the first study was to determine if diffusion abnormality was also present in the contralateral NAWM of patients with non-infiltrative tumors such as meningiomas.

The secondary aim was to search for other possible factors that could contribute to ADC elevation in the contralateral NAWM. Since a certain amount of mass effect is present in tumors regardless of their infiltrative or non-infiltrative behavior, the further purpose of the study was to investigate its role in causing contralateral NAWM diffusion abnormalities.

The goal of the second study was to further clarify the nature of elevated ADC in NAWM of glioma patients with the more detailed biexponential diffusion analysis and to reveal if the observed diffusion alterations were region specific or global.

3. Methods

3.1 Increased diffusion in the normal appearing white matter of brain tumor patients: is this just tumor infiltration?

3.1.1 Patients

Inclusion criteria were newly diagnosed grade II-IV gliomas and grade I-II meningiomas with MRI scans before any intervention, surgery or treatment and age older than 18. Forty-two glioma and 25 meningioma patients were initially enrolled in this retrospective study.

Two patients were excluded because of recurrent tumor, one patient was excluded because of previous radiation therapy, eight patients were excluded because the white matter contralateral to the tumor was affected by the tumor, or contralateral white matter showed hyperintense signal abnormalities on T2-weighted scans, five patients were excluded due to bad image quality, one patient was excluded due to other malignant disease, and one patient was excluded due to psychiatric illness.

After exclusions, 49 patients remained. Twenty-seven patients had gliomas (13 females, 14 males; mean age: 49.0 ± 16.9 years), and 22 patients had meningiomas (15 females, 7 males; mean age: 53.5 ± 12.3 years). Imaging was performed before any intervention or treatment in all patients. Afterwards, histopathologic diagnosis was based on surgically resected or biopsied tissues. Eleven patients had grade II gliomas (5 diffuse astrocytomas, 4 oligodendrogliomas and 2 oligoastrocytomas), three had grade III gliomas (2 anaplastic astrocytomas, 1 anaplastic oligodendroglioma) and thirteen had grade IV glioblastomas. Grade II gliomas were considered as low grade, while grade III and IV gliomas were considered as high grade. Among the meningioma patients, 20 had grade I and 2 had grade II meningiomas.

3.1.2 Control subjects

Twenty-seven age and sex matched healthy subjects served as a control group for the glioma patients (mean age: 49.0 ± 19.4 years) and 22 age and sex matched healthy subjects (mean age: 53.1 ± 12.6 years) were enrolled as a control group for the meningioma patients.

3.1.3 Magnetic Resonance Imaging

MR imaging was performed on a 3 T Siemens TIM Trio MRI scanner (Siemens AG, Erlangen, Germany) with a 12-channel head coil. Conventional anatomical imaging included T1-, T2-weighted, and FLAIR sequences.

Three-dimensional T1-weighted post-contrast MPRAGE images (TR/TI/TE = 2530/1100/3.37 ms, flip angle 7°, 176 sagittal slices, slice thickness 1 mm, field of view 256 x 256 mm^2, matrix 256 x 256, receiver bandwidth 200 Hz/pixel, GRAPPA 2) served as structural scans in patients.

Three-dimensional T1-weighted MPRAGE images (TR/TI/TE = 1760/900/3.41 ms, flip angle 9°, 120 axial slices, slice thickness 1.5 mm, field of view 180 x 230 mm^2, matrix 192 x 256, receiver bandwidth 180 Hz/pixel, GRAPPA 2) served as structural scans in control subjects.

For DWI, a spin-echo echo-planar sequence (TR/TE = 3800/91 ms, 75 axial slices, slice thickness 3.5 mm, no gap, field of view 219 x 250 mm^2, matrix 168 x 192, bandwidth 1240 Hz/pixel, b factors: 0, 500, 1000 s/mm^2) was used in all patients and control subjects.

3.1.4 Image analysis

Image analysis was performed by A. H. while blinded to the results of histology. The entire NAWM in the hemisphere contralateral to the tumor was automatically segmented on MPRAGE images with Freesurfer software (Fischl et al., 2002). In control subjects, the corresponding NAWM was segmented (as in the age- and sex-matched patients).

MPRAGE images were then registered to diffusion weighted scans (6 degrees-of-freedom linear fit, correlation ratio cost function and trilinear interpolation) using FSL FLIRT (FMRIB's Linear Image Registration Tool) (Jenkinson et al., 2002). Then, the spatial transform of the MPRAGE-to-diffusion co-registration was used to align the segmented NAWM masks to the diffusion space (trilinear interpolation).

The resulting masks were thresholded using a 0.9 threshold to avoid partial volume effects and to minimize possible impacts of misalignment between NAWM masks and diffusion weighted images. Masks were manually corrected to exclude

any non-white matter structure especially in the inferior part of the temporal and frontal lobes, which are prone to susceptibility artifacts.

ADC values in the NAWM were calculated by fitting the monoexponential signal decay over b values using Eq. (3), see page 11. Curve fitting was performed using Matlab software (MathWorks, Natick, MA).

In order to assess the influence of mass effect on ADC values of the contralateral NAWM, tumor volumes in both patient groups were measured by manually delineating the tumors on all slices where it was visible on the MPRAGE images using 3D Slicer software package (Fedorov et al., 2012). Although FLAIR or T2-weighted images provide better visualization of tumor extent, T1-weighted MPRAGE scans had a better resolution which enabled more accurate volumetry. For this reason, tumor volumes were measured on MPRAGE images but the corresponding areas were visually checked on T2-weighted scans. In grade II gliomas, tumor and edema could not be clearly distinguished. In order to standardize volumetry in all glioma grades, edema and tumor were marked in one label called `tumor` in all gliomas. In meningiomas both a tumor only and a tumor + edema label were created. These tumor masks were not used to calculate ADC. A representative image of the analysis process is shown in Fig. 14.

3.1.5 Statistical analysis

Statistical analyses were performed using SPSS 20.0 software (IBM Corp., Armonk, NY). Comparisons between patient and control groups were performed by two tailed Mann–Whitney U–tests.

Considering age-related ADC differences, each comparison was repeated by creating a multiple linear regression model with mean ADC as dependent, while group membership (patient vs. control) and age as independent variables. ADC values of the NAWM between high grade gliomas and low grade gliomas were compared with the same model.

The assumptions of multiple linear regression were satisfied, as judged by testing for linearity, normality assumptions of the residues, outliers, independence of errors, homoscedasticity and multi-collinearity (Brugieres et al., 2004).

In order to investigate the relationship between the measured contralateral NAWM ADC values and tumor volume, multiple linear regression was performed

with mean ADC as dependent while age, tumor volume - and in the case of gliomas - tumor grade as independent variables. Results were considered significant, if $P < 0.05$.

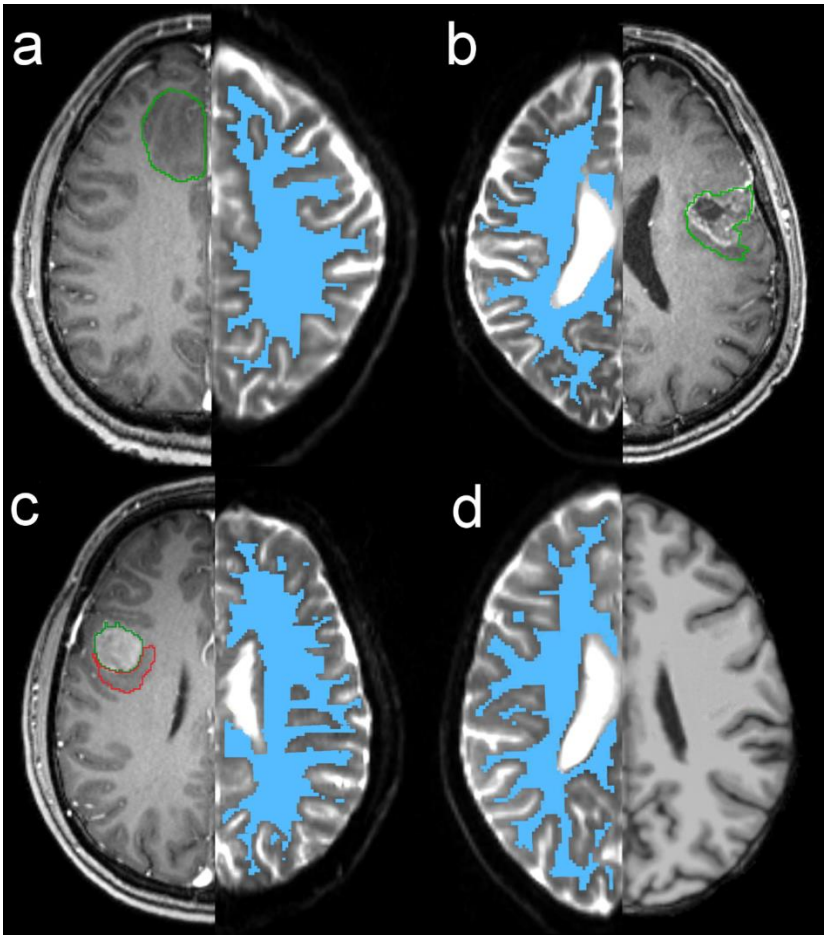

Fig. 14. Representation of the analysis process. An example of a T1-weighted MPRAGE image co-registered to the b0 image of a a) grade II glioma patient (left and right, respectively), b) grade IV glioma patients (right and left, respectively), c) meningioma patient (left and right, respectively) and d) healthy control subject (right and left, respectively) are shown. The NAWM mask, that was originally segmented on MPRAGE images and was used to extract mean ADC values, can be seen after co-registration, thresholding and manual correction in the space of DWI (blue color). The green line indicates the region of interest that was used to measure tumor volume in gliomas and meningiomas. The red line indicates the ROI placed on the edema in meningioma patients only. In meningiomas, tumor + edema volume was calculated by adding the volume of ROIs delineated by the green and red lines. Volumetry was performed on unregistered MPRAGE images.

3.2 Biexponential diffusion alterations in the normal appearing white matter of glioma patients might indicate the presence of global vasogenic edema

3.2.1 Subjects

This prospective study was approved by the Regional Research Ethics Committee. All subjects gave written informed consent before the examination.

Inclusion criteria were newly diagnosed, unilateral grade II-IV gliomas with MRI scans before any intervention or treatment (surgery, chemoradiation) and age older than 18 years. Thirty patients were initially enrolled in the study. Three patients were excluded because white matter contralateral to the tumor showed hyperintense signal abnormalities on T2-weighted scans and three patients were excluded due to unavailable histology.

After exclusions, 24 patients with newly diagnosed, histologically verified glioma remained in the study. Patient characteristics are described in Table 2.

Table 2. Patient demographics, tumor histology and tumor locations.

Patient characteristics	
Mean age ± SD (years)	42.29 ± 11.44
Gender distribution	14M, 10F
Histology	
Grade II (n=13)	DA: 4, OD: 7, OA: 1, GA: 1
Grade III (n=4)	AA: 2, AOA: 1, AOD: 1
Grade IV (n=7)	GBM: 7
Tumor affected lobes	
Frontal	11
Parietal	7
Occipital	6
Temporal	2

SD: standard deviation, M: male, F: female, DA: diffuse astrocytoma, OD: oligodendroglioma, OA: oligoastrocytoma, GA: gemistocytic astrocytoma, AA: anaplastic astrocytoma, AOA: anaplastic oligoastrocytoma, AOD: anaplastic oligodendroglioma, GMB: glioblastoma

As a control group, twenty-four age and gender matched healthy control subjects (14 males, 10 females, mean age ± SD: 42.08 ± 10.94 years, age range: 23-63 years) were included.

3.2.2 Magnetic Resonance Imaging

MR imaging was performed on a 3T Siemens TIM Trio MRI scanner (Siemens AG, Erlangen, Germany) with a 12-channel head coil. Conventional anatomical imaging included T1-, T2-weighted, and FLAIR sequences.

Three-dimensional T1-weighted MPRAGE images (TR/TI/TE: 2530/1100/3.37 ms, flip angle 7°, 176 sagittal slices, slice thickness 1 mm, field of view 256 x 256 mm^2, matrix 256 x 256, receiver bandwidth 200 Hz/pixel, GRAPPA 2) served as structural scans.

For diffusion weighted imaging, a 2D trace-weighted single shot echo planar imaging sequence (TR/TE: 4800/128 ms, slice thickness 3.5 mm, distance factor 30%, field of view: 188 x 250 mm^2, matrix 144 x 192, number of acquisitions: 5, b-values: 0, 500, 1000, 2000, 3000, 4000, 5000 s/mm^2) was used.

3.2.3 Image analysis

Image analysis was performed by A. H. while blinded to the results of histology. The entire white matter (WM) in the hemisphere contralateral and ipsilateral to the tumor was automatically segmented on MPRAGE images using Freesurfer software (Fischl et al., 2002). Besides the entire contralateral and ipsilateral hemispheric WM masks, regional regions of interest (ROIs) were also created by automatically parcellating the contralateral WM into frontal, parietal, occipital and temporal lobe regions in each subject.

In control subjects, the corresponding WM regions were segmented (as in the age- and sex-matched patients).

MPRAGE images were then registered to diffusion weighted scans (6 degrees-of-freedom linear fit, correlation ratio cost function and trilinear interpolation) using FSL FLIRT (FMRIB's Linear Image Registration Tool) (Jenkinson et al., 2002). Then, the matrix of the MPRAGE-to-diffusion co-registration was used to align the segmented binary WM masks to the diffusion space (trilinear interpolation).

The resulting total contralateral and ipsilateral hemispheric WM masks were thresholded using a 0.9 threshold to avoid partial volume effects and to minimize possible impacts of misalignment between WM masks and diffusion weighted images. All ROIs (regional and total hemispheric masks) were manually corrected to exclude any non-white matter structure especially in the inferior part of the temporal and frontal lobes which are prone to susceptibility artifacts, or any white matter hyperintensities visible on T2-weighted scans (i.e. b=0 s/mm^2). Attention was paid to avoid any tumor and edema containing regions especially in the ipsilateral WM ROIs. The resulting ROIs were defined as NAWM masks.

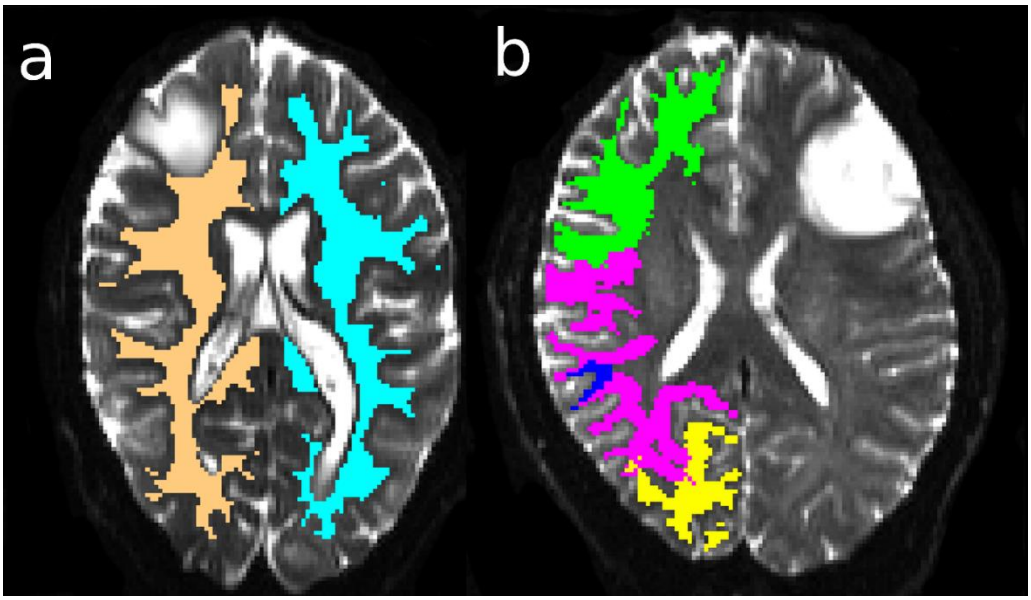

Fig. 15. Normal appearing white matter (NAWM) region of interests (ROIs). a) Diffusion weighted image acquired with b=0 s/mm2 of a low grade glioma patient with the total contralateral hemispheric normal appearing white matter (NAWM) region of interest (ROI) (light blue) and the total ipsilateral hemispheric NAWM ROI (copper). b) Diffusion weighted image acquired with b=0 s/mm2 of a low grade glioma patient with the regional NAWM ROIs in the hemisphere contralateral to the tumor. Green: frontal NAWM, magenta: parietal NAWM, blue: temporal NAWM, yellow: occipital NAWM.

Diffusion parameters were assessed in all ROIs of patients and control subjects. ADC_{mono} values were calculated by fitting the monoexponential signal decay over the low b-value range (i.e., b-values of 0, 500, and 1000 s/mm^2) using

Eq. (3), see page 11. ADC values were broken down into ADC_{fast} and ADC_{slow} by applying the biexponential fit in the whole b-value range (i.e. 0- 5000 s/mm^2) using Eq. (4), see page 14. Curve fitting was performed using Matlab software's curve fitting toolbox and an in-house program code (MathWorks, Natick, MA).

Fig. 15. Illustrates hemispheric and reginal NAWM masks.

3.2.4 Statistical analysis

Statistical analyses were performed using SPSS 20.0 software (IBM Corp., Armonk, NY). Normality of data distribution was tested by Shapiro-Wilk statistics. Homogeneity of variance was assessed by Levene's test. Both total hemispheric and regional diffusion values were compared between patient and control groups by Student's t test or two tailed Mann–Whitney–U test according to the statistical distribution of the data. In order to control for the potential confounding effects of age, each comparison was repeated by creating a multiple linear regression model including age as a covariate. Gliomas might spread into the mirror regions of the contralateral hemisphere through the corpus callosum (Kallenberg et al., 2013). Therefore, to control for the potential confounding effect of tumor location, the multiple linear regression model included tumor location as an additional covariate besides age in the regional analysis; tumor location was handled as a binary variable (present or absent) in the analysis of each lobe. The assumptions of multiple linear regression were satisfied, as judged by testing for linearity, normality assumptions of the residues, outliers, independence of errors, homoscedasticity and multi-collinearity (Chan, 2004).

Two-way mixed ANOVA was performed to evaluate whether regional differences in diffusion parameters were significant between patients and controls. The same analysis was used to assess whether hemispheric differences in diffusion values are the same in patients and controls.

Results were considered significant, if $P < 0.05$.

4. Results

4.1 Increased diffusion in the normal appearing white matter of brain tumor patients: is this just tumor infiltration?

Demographic data of subject groups and mean ADC values measured in the contralateral NAWM are presented in Table 3.

Table 3. Demographic data and mean ADC values measured in contralateral NAWM

Subject group	Mean age ± SD (years)	Gender distribution	ADC ($10^{-4}mm^2/s$)
Glioma patients	49.0 ± 16.9	13 F, 14 M	7.99 ± 0.54
HC for gliomas	49.0 ± 19.4	13 F, 14 M	7.67 ± 0.29
Meningioma patients	53.5 ± 12.3	15 F, 7 M	7.90 ± 0.23
HC for meningiomas	53.1 ± 12.6	15 F, 7 M	7.73 ± 0.24
HGG	54.8 ± 18.6	7 F, 9 M	8.25 ± 0.54
HC for HGGs	54.1 ± 18.8	7 F, 9 M	7.74 ± 0.32
LGG	40.5 ± 9.7	6 F, 5 M	7.61 ± 0.25
HC for LGGs	41.8 ± 8.5	6 F, 5 M	7.58 ± 0.21

ADC: apparent diffusion coefficient in the normal appearing white matter, F: female, M: male, HC: healthy controls, HGG: high grade glioma, LGG: low grade glioma

Significantly elevated ADC values were found in the contralateral NAWM of glioma patients ($7.99 \pm 0.54 \cdot 10^{-4}mm^2/s$ [mean ± SD]) compared to control subjects ($7.67 \pm 0.29 \cdot 10^{-4}mm^2/s$) with Mann–Whitney U–test ($P = 0.0326$; Fig. 16a). ADC values were significantly higher in the contralateral NAWM of meningioma patients ($7.90 \pm 0.23 \cdot 10^{-4}mm^2/s$) compared to healthy controls ($7.73 \pm 0.24 \cdot 10^{-4}mm^2/s$) shown by Mann–Whitney U–test ($P = 0.0098$; Fig. 16a). The results of the comparisons remained significant after adjusting for age with the multiple linear regression model ($P = 0.0006$ and $P = 0.0099$, respectively).

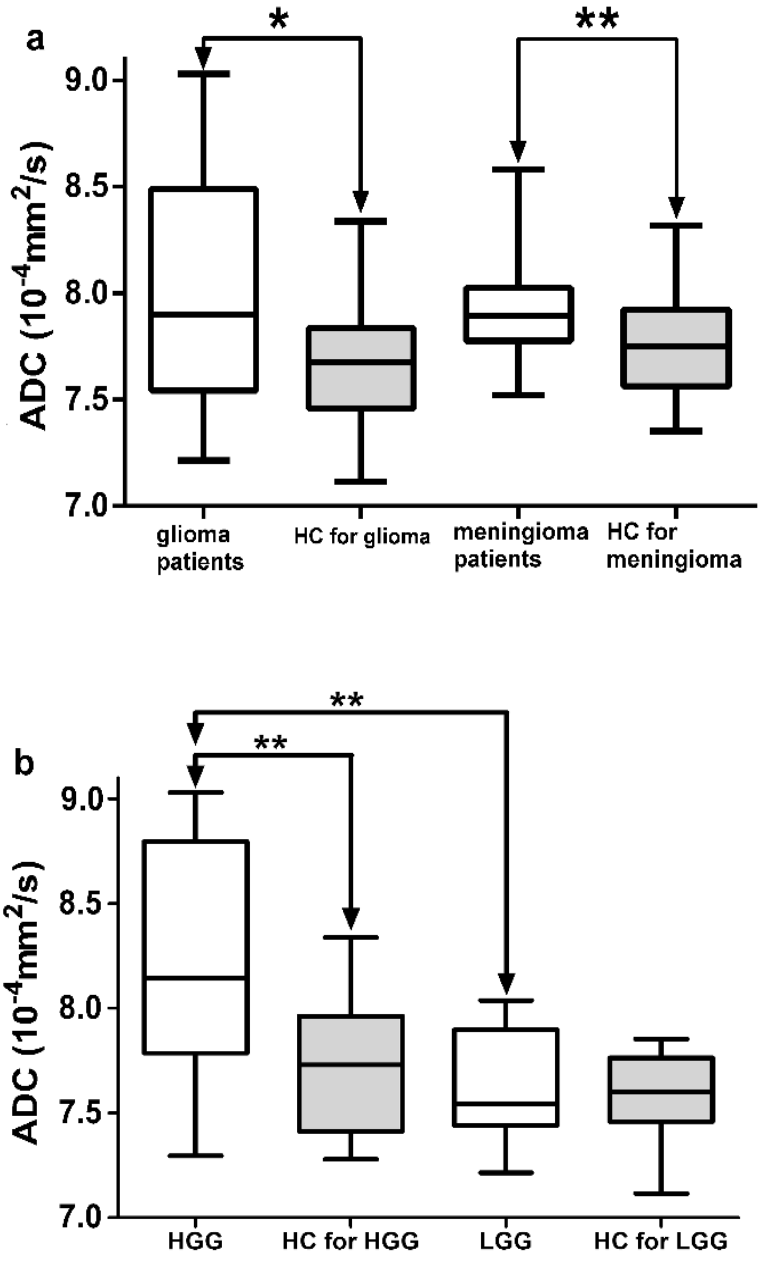

Fig. 16. Comparisons of ADC values in the contralateral NAWM. a) Boxplot illustrating the significantly increased ADC in the contralateral NAWM of glioma and meningioma patients compared with healthy control subjects. b) Boxplot illustrating the significantly increased ADC in the contralateral NAWM of high grade glioma patients compared with healthy control subjects and low grade glioma patients. Whiskers are set at minimum and maximum, the horizontal line marks the median, whereas box indicates the interquartile range (25-75%). * indicates $P<0.05$, ** indicates $P<0.01$. HC: healthy control.

In glioma patients, ADC was significantly higher in the contralateral NAWM of high grade glioma patients ($8.25 \pm 0.54 \cdot 10^{-4} mm^2/s$) than in that of low grade glioma patients ($7.61 \pm 0.25 \cdot 10^{-4} mm^2/s$) with Mann–Whitney U–test (P = 0.0019; Fig. 16b). Comparing high grade glioma patients to matched control subjects, ADC values in the contralateral NAWM were elevated with Mann–Whitney U–test (P = 0.0083; Fig. 16b). These differences remained significant after adjusting for age with the multiple linear regression model (P = 0.0003). On the other hand, the contralateral NAWM of low grade glioma patients did not show significantly different ADC values compared to matched healthy subjects neither with Mann–Whitney U–test nor with the multiple linear regression model (P = 0.8696 and P = 0.5445, respectively). The summary of ADC value comparisons between groups is presented in Table 4.

Table 4. Comparisons of ADC values in the contralateral NAWM between groups.

Comparisons	Mann–Whitney U–test	Multiple linear regression
Glioma vs. Healthy controls	P = 0.0326	P = 0.0006[a]
Meningioma vs. Healthy controls	P = 0.0098	P = 0.0099[a]
HGG vs. LGG	P = 0.0019	P = 0.0181[a]
LGG vs. Healthy controls	NS	NS[a]
HGG vs. Healthy controls	P = 0.0083	P = 0.0003[a]

[a]Multiple linear regression with adjustment for age

NS: statistically not significant (P>0.05), HGG: high grade glioma, LGG: low grade glioma

Tumor volume was $51.56 \pm 44.01 cm^3$ in gliomas (mean ± SD) and $34.02 \pm 33.65 cm^3$ in meningiomas. Tumor + edema volume was $47.39 \pm 45.01 cm^3$ in meningiomas. ADC values in the contralateral NAWM were not dependent on tumor volume neither in the glioma (P = 0.7489) nor in the meningioma group (P = 0.4750). ADC values did not depend on tumor + edema volume in the meningioma group (P = 0.8258).

4.2 Biexponential diffusion alterations in the normal appearing white matter of glioma patients might indicate the presence of global vasogenic edema

4.2.1 Comparison of patients with controls

4.2.1.1 Hemispheric analysis

Table 5 and Fig. 17 present the mean diffusion values in both total hemispheric NAWM of both groups. In the contralateral hemispheric NAWM, ADC_{mono}, ADC_{fast} and ADC_{slow} were significantly higher ($P < 0.0001$, $P = 0.0071$ and $P = 0.0255$, respectively), while p_{slow} was significantly lower ($P = 0.0061$) in the patient group compared to controls. In the hemisphere ipsilateral to the tumor, ADC_{mono} and ADC_{fast} were significantly higher, and p_{slow} was significantly lower ($P = 0.0013$, $P = 0.0372$ and $P = 0.0011$ respectively) in the NAWM of glioma patients compared to control values. ADC_{slow} in the total NAWM ipsilateral to the tumor did not show any difference between the two groups ($P = 0.9351$).

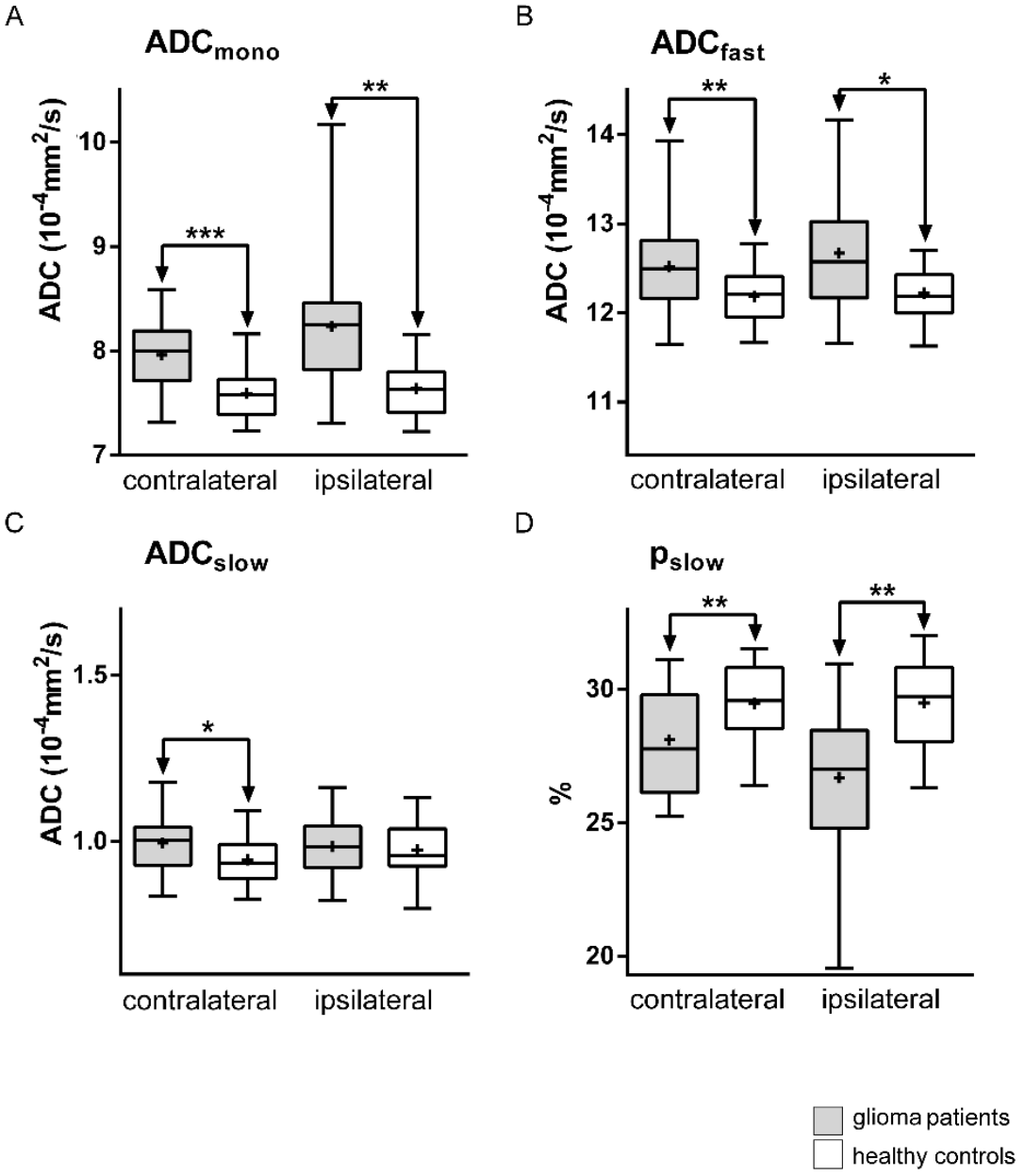

Fig. 17. Results of the comparisons of monoexponential ADC_{mono} (A), biexponential ADC_{fast} (B), ADC_{slow} (C) and p_{slow} (D) values in the NAWM of glioma patients and healthy controls. In the boxplots, whiskers are set at minimum and maximum, the horizontal line marks the median, + indicates the mean, whereas box indicates the interquartile range (25-75%). * indicates P<0.05, ** indicates P<0.01, *** indicates P<0.001 Contralateral and ipsilateral indicate the total NAWM in the hemisphere contralateral and ipsilateral to the tumor.

Table 5. Mean diffusion values ± SD ($10^{-4}mm^2/s$) in the normal appearing white matter and results of the statistical comparisons of patient and control subjects.

Locations		groups	ADC_{mono}	p value	ADC_{fast}	p value	ADC_{slow}	p value	p_{slow} (%)	p value
contralateral		*patients*	7.96 ± 0.32	**< 0.0001***	12.52 ± 0.50	**0.0071***	1.00 ± 0.09	**0.0255***	28.11 ± 1.93	**0.0061***
		controls	7.59 ± 0.23		12.18 ± 0.31		0.95 ± 0.07		29.47 ± 1.47	
ipsilateral		*patients*	8.24 ± 0.62	**0.0013***	12.67 ± 0.71	**0.0372***	0.99 ± 0.09	0.9351*	26.70 ± 2.82	**0.0011***
		controls	7.64 ± 0.24		12.25 ± 0.28		0.97 ± 0.08		29.46 ± 1.71	
contralateral	frontal	*patients*	8.01 ± 0.32	**0.0002†**	12.24 ± 0.61	**0.0306†**	1.06 ± 0.11	**0.0026†**	26.90 ± 1.87	0.0645†
		controls	7.56 ± 0.32		11.63 ± 0.62		0.92 ± 0.12		27.04 ± 1.86	
	parietal	*patients*	8.27 ± 0.39	**0.0002†**	12.52 ± 0.56	**0.0053†**	1.20 ± 0.16	**0.0195†**	26.61 ± 1.75	**0.0312†**
		controls	7.82 ± 0.27		12.11 ± 0.44		1.10 ± 0.14		28.07 ± 1.44	
	occipital	*patients*	8.33 ± 0.43	**0.0004†**	12.77 ± 0.69	**0.0056†**	1.20 ± 0.20	0.1130†	27.03 ± 1.90	0.2391†
		controls	7.90 ± 0.30		12.20 ± 0.64		1.11 ± 0.15		27.70 ± 1.69	
	temporal	*patients*	8.21 ± 0.39	0.0859†	12.16 ± 0.60	0.3936†	1.00 ± 0.18	0.1747†	24.88 ± 1.69	0.1482†
		controls	7.95 ± 0.42		11.97 ± 0.67		0.92 ± 0.17		25.80 ± 1.57	

SD: standard deviation, ADC_{mono}: apparent diffusion coefficient, ADC_{fast}: ADC of the fast diffusion component, ADC_{slow}: ADC of the slow diffusion component, p_{slow}: volume fraction of the slow diffusion component. Significant results are marked with bold font.

*Multiple linear regression with adjustment for age

†Multiple linear regression with adjustment for age and tumor location

4.2.1.2 Regional NAWM analysis

Table 5 and Fig. 18 present the mean diffusion values of the contralateral NAWM regions in both groups. The regional analysis of the NAWM contralateral to the tumor revealed significantly increased ADC_{mono} and ADC_{fast} values in the frontal ($P = 0.0002$ and $P = 0.0306$, respectively), parietal ($P = 0.0002$ and $P = 0.0053$, respectively) and occipital ($P = 0.0004$ and $P = 0.0056$, respectively) NAWM regions of glioma patients compared to healthy subjects. ADC_{slow} was significantly higher in the frontal ($P = 0.0026$) and parietal ($P = 0.0195$) lobes of glioma patients compared to healthy subjects, while p_{slow} was significantly decreased in the contralateral parietal NAWM of glioma patients compared to controls ($P = 0.0312$).

In the occipital NAWM, ADC_{slow} and p_{slow} did not differ between patients and controls ($P = 0.1130$ and $P = 0.2391$, respectively). None of the diffusion parameters showed significant difference between patients and controls in the temporal NAWM ($P > 0.05$).

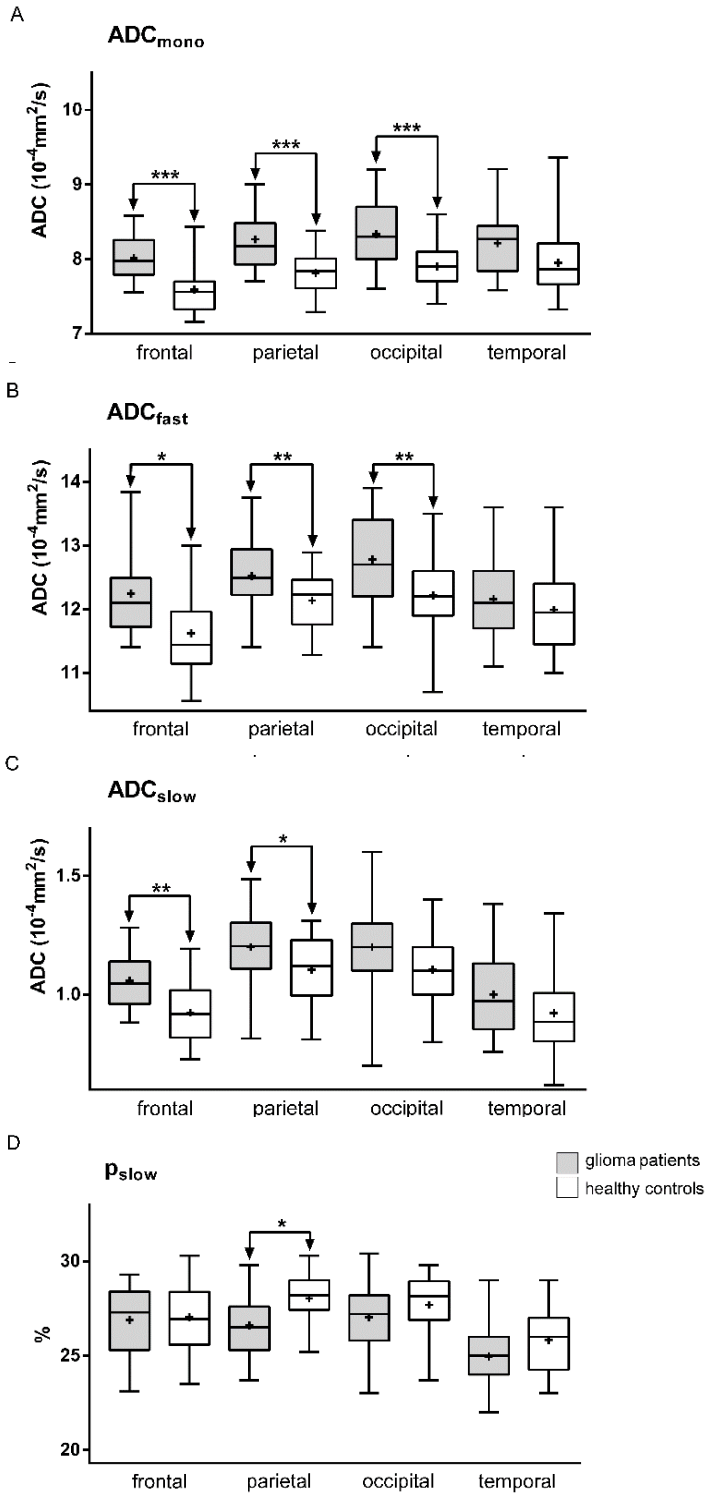

Fig. 18. Results of the comparisons of monoexponential ADC_{mono} values (A) and the biexponential ADC_{fast} (B), ADC_{slow} (C) and p_{slow} (D) values in the contralateral NAWM of glioma patients and healthy controls. In the boxplots, whiskers are set at minimum and maximum, the horizontal line marks the median, + indicates the mean, whereas box indicates the interquartile range (25-75%). * indicates P<0.05, ** indicates P<0.01, *** indicates P<0.001 Frontal, parietal, occipital and temporal indicate the regional NAWM ROIs in the hemisphere contralateral to the tumor.

4.2.2 Comparison of diffusion parameters among hemispheres and regions

4.2.2.1 Hemispheric analysis

The results of hemispheric analysis with two-way mixed ANOVA are presented in Table 6.

Table 6. P values of hemispheric analysis with two-way mixed ANOVA

	group	hemisphere	group*hemisphere
ADC_{mono}	<0.0001	0.0076	0.0407
ADC_{fast}	0.0065	NS	NS
ADC_{slow}	NS	NS	NS
p_{slow}	0.0010	0.0003	0.0005

NS: not significant. ADC_{mono}: apparent diffusion coefficient, ADC_{fast}: ADC of the fast diffusion component, ADC_{slow}: ADC of the slow diffusion component, p_{slow}: volume fraction of the slow diffusion component, group: between subject variable (i.e. patient or control), hemisphere: within subject variable (i.e. contralateral or ipsilateral NAWM), group*hemisphere: interaction between group and diffusion parameters

ADC_{mono} and p_{slow} in the NAWM was significantly different between both hemispheres (P = 0.0076 and P = 0.0003, respectively). ADC_{fast} and ADC_{slow} did not differ between the two hemispehere's NAWM. The significant group*hemisphere interactions in ADC_{mono} and p_{slow} analyses (P = 0.0407 and P = 0.0005, respectively) indicate that the ADC_{mono} and p_{slow} differences between the NAWM of the two hemispheres change differently in the two groups.

4.2.2.2 Regional analysis

The results of regional analysis with two-way mixed ANOVA are presented in Table 7.

Table 7. P values of the regional two-way mixed ANOVA analysis and results of the post hoc test (presented P values are Bonferroni corrected).

	two-way mixed ANOVA			Post hoc test†					
	group	region	group*region	frontal vs. parietal	frontal vs. occipital	frontal vs. temporal	parietal vs. occipital	parietal vs. temporal	occipital vs. temporal
ADC_{mono}	0.0002	<0.0001	NS	<0.0001	<0.0001	<0.0001	NS	NS	NS
ADC_{fast}	0.0027	<0.0001	NS	0.0006	<0.0001	NS	NS	0.0198	0.0001
ADC_{slow}	0.0069	<0.0001	NS	<0.0001	<0.0001	NS	NS	<0.0001	<0.0001
p_{slow}	NS	<0.0001	0.0381	NS	NS	<0.0001	NS	<0.0001	<0.0001

NS: not significant. ADC_{mono}: apparent diffusion coefficient, ADC_{fast}: ADC of the fast diffusion component, ADC_{slow}: ADC of the slow diffusion component, p_{slow}: volume fraction of the slow diffusion component. Group: between subject variable (i.e. patient or control), region: within subject variable (i.e. frontal, parietal, temporal or occipital normal appearing white matter of the hemisphere contralateral to the tumor), group*region: interaction between group and diffusion parameters.

†Presented P values are Bonferroni corrected)

In the regional analysis of the NAWM in the hemisphere contralateral to the tumor, significant difference was observed in all four diffusion parameters among regions ($p<0.0001$). ADC_{mono} in the frontal NAWM was significantly lower than all other regions (<0.0001, Bonferroni correction). ADC_{fast} and ADC_{slow} in the frontal and temporal NAWM was significantly lower than in the occipital and parietal NAWM ($P < 0.05$, Bonferroni correction). P_{slow} in the temporal NAWM was significantly lower than all other regions ($P < 0.0001$, Bonferroni correction).

There was no significant group*region interactions in the ADC_{mono}, ADC_{fast} and ADC_{slow} analyses (i.e. regional diffusion differences were the same in patients and in controls). Significant group*region interaction in the p_{slow} analysis indicates that changes in p_{slow} among NAWM regions were different in patients and controls ($p=0.0381$).

5. Discussion

5.1 Increased diffusion in the normal appearing white matter of brain tumor patients: is this just tumor infiltration?

Diffusion abnormalities have been previously observed in the NAWM of glioma patients, and these findings were explained with the presence of infiltrative tumor cells. The goal of the present study was to test this explanation indirectly by examining if these alterations were also present in the NAWM of non-infiltrative tumors like meningiomas; and to draw attention to the other possible mechanisms that could lead to ADC elevation in the NAWM of brain tumor patients. This study demonstrated that ADC measured in the contralateral NAWM of meningioma patients was increased in a similar fashion as it had been previously reported in glioma patients. Since meningiomas are well-circumscribed tumors, ADC elevation in the contralateral NAWM cannot be caused by tumor infiltration.

Our results are in agreement with the finding of Inglese et al. (Inglese et al., 2006) and Kallenberg et al. (Kallenberg et al., 2014), who found increased ADC in the contralateral NAWM of glioma patients. Although Inglese et al. mention blood brain barrier disturbance resulting from tumor growth as a possible reason for ADC elevation, both study conclude that this alteration is a result of possible tumor infiltration. Similarly to Maudsley et al. (Maudsley et al., 2013), we also found elevated mean diffusivity in the contralateral NAWM of glioma patients which correlated with tumor grade. The study of Inglese et al. and Maudsley et al. included whole-brain MR spectroscopy as well, and the global N-acetylaspartate loss was interpreted as a result of cytokines produced by the tumor cells. Besides the low number of patients investigated, the limitation of the study of Inglese et al. is that the control group was not age and sex matched, and no adjustment was performed for age, although ADC of white matter depends on age (Nagy et al., 2013a). The drawback of the study of Maudsley et al. is that control subjects were not matched, and the differences resulting from the different MRI scanners used for the examination of the patients and controls might have had an influence on the results. In all of these three studies ADC was calculated from a manually placed region of interest from a single slice only.

Water diffusion in the brain is affected by tissue microstructure, therefore ADC can be used to monitor changes related to different pathologies. Increased

ADC values can be observed when diffusion becomes less restricted. There might be many possible mechanisms that could contribute to elevated ADC. ADC shows a gradual increase with age (Naganawa et al., 2003). Besides this, the increase of ADC in the NAWM has been previously observed in other diseases such as multiple sclerosis (Nagy et al., 2013a, Orsi et al., 2014), where the abnormality was explained by the loss of myelin sheath and in glioma patients (Inglese et al., 2006, Maudsley et al., 2013, Kallenberg et al., 2014), where it was explained by the effect of infiltrative tumor cells.

How can tumor infiltration cause higher ADC? Based on studies measuring diffusion in the peritumoral region of patients with glioma, meningioma and brain metastasis (Lu et al., 2003, Provenzale et al., 2004, Morita et al., 2005, Toh et al., 2007, Romano et al., 2008, Bieza and Krumina, 2012), tumor cells can either dislocate nerve fibers or destroy white matter (Inglese et al., 2006, Kallenberg et al., 2014) resulting in increased ADC. White matter tracts may be destroyed (Lu et al., 2003, Provenzale et al., 2004, Toh et al., 2007, Romano et al., 2008) directly by the invasion of tumor cells (Inglese et al., 2006, Kallenberg et al., 2014), or indirectly by the secretion of cytotoxic substances (Toh et al., 2007). Infiltrating glioma cells can also destroy extracellular matrix of the brain through their proteolytic activity (Morita et al., 2005). White matter and extracellular matrix degradation both result in more extracellular space which is less obstructive to water. These factors add to the effect of vasogenic edema which is called infiltrative edema by some authors (Cha, 2006). The drawback of these studies was that instead of comparing peritumoral mean diffusivity values to values from normal white matter areas of healthy control subjects, they all compared them to that of the contralateral NAWM. Mean diffusivity in the contralateral NAWM differs from normal which makes the interpretation of the results difficult.

Since ADC values were increased in the NAWM of patients with non-infiltrative tumors as well, it may seem likely that there are other factors besides tumor infiltration that contribute to increased ADC in the NAWM of brain tumor patients. It would seem to be logical to explain these findings with mechanisms that are present in both infiltrative and non-infiltrative tumor patients.

Both gliomas and meningiomas compress their surroundings. Tumor compression could lead to venous congestion and disturbance of microcirculation (Toh et al., 2007), thus increased ADC in the contralateral NAWM could be a result

of mass effect. There are several methods to characterize mass effect, including measurement of midline shift, tumor diameter or tumor volume. Since the latter one seemed to be the most objective approach, we measured the tumor volumes and investigated their relationship to ADC values in the contralateral NAWM. However, this hypothesis was not proved by our results, since ADC values were not related to tumor volume either with or without edema. Even if it remains hypothetic, a possible explanation might be that ADC elevation depends on tumor growth rate, or ADC increases due to mass effect only until it reaches a limit.

Considering other common characteristics of gliomas and meningiomas, both tumors imply the secretion of substances such as VEGF (Tsai et al., 2003, Toh et al., 2007, Nassehi, 2013a) and cytokines (Van Meir et al., 1990, Black et al., 1992, Todo et al., 1994) which could affect the brain globally. VEGF increases the permeability of the blood brain barrier (Mayhan, 1999), that results in extracellular fluid accumulation. Plasma fluid escaping the vessels produces vasogenic edema (Lu et al., 2003, Pauleit et al., 2004, Provenzale et al., 2004, Morita et al., 2005) that leads to increased ADC. Pro-inflammatory citokynes such as IL-6 and TNF-α might have an effect on microvascular endothelial cells possibly by dysregulating the interendothelial paracellular pathway (Rochfort and Cummins, 2015). This can lead to increased blood brain barrier permeability (Rochfort and Cummins, 2015) resulting in increased ADC. Although this hypothetic mechanism of action of VEGF and cytokines is based on literature data, Fig. 19. summarizes the possible factors that might contribute to ADC elevation in the contralateral NAWM of brain tumor patients.

These possible differences in the pathomechanism might explain the differences in the magnitude of ADC elevation in the NAWM of patients with different tumor types. The presence of increased ADC values in the contralateral NAWM of both infiltrative and non-infiltrative tumor patients may indicate that mechanisms present in both groups (e.g. VEGF secretion, cytokine secretion) may contribute to elevated ADC. Conversely, it is also possible, that ADC elevation in the contralateral NAWM is the result of completely different mechanisms in this two tumor groups.

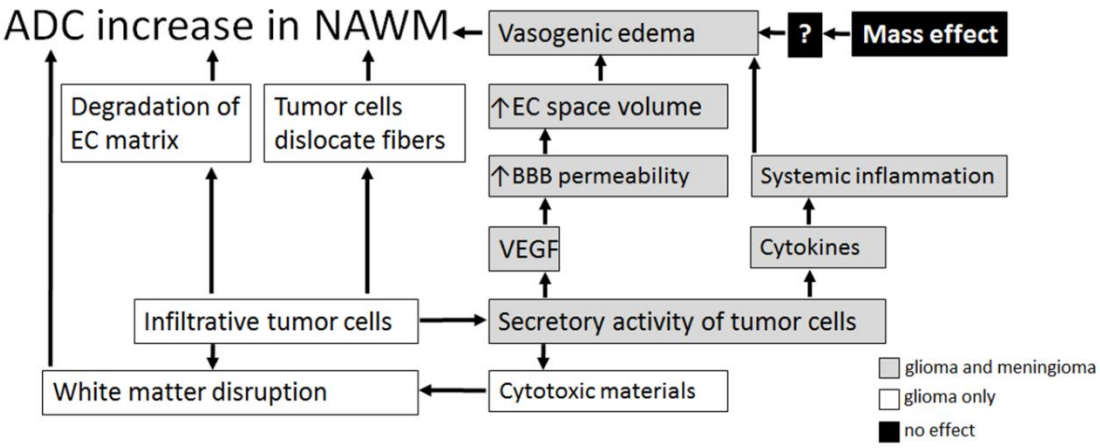

Fig. 19. Summary of possible factors based on literature data that could contribute to ADC elevation in the NAWM. Grey boxes: factors possibly present in both gliomas and meningiomas. White boxes: factors that might only be present in infiltrating tumors such as gliomas. Black boxes: factors whose contribution to increased ADC appears unlikely based on our results. Abbreviations: EC: extracellular, BBB: blood brain barrier. VEGF: vascular endothelial growth factor.

Nevertheless, higher ADC values were found in the NAWM of high grade glioma patients than in that of low grade glioma patients. The dependence of ADC values of NAWM on glioma grade can be explained by the fact that although low grade gliomas are known to be infiltrative, in the early stages the contralateral NAWM might be less affected.

To prove the direct relationship of increased ADC and tumor infiltration in vivo in the human NAWM is experimentally challenging. Nevertheless, it might be possible by specifically labeling and visualizing infiltrating tumor cells with sufficient sensitivity (e.g. with PET imaging). Although it is possible to perform diffusion weighted imaging in post mortem or formalin-fixed brains, ADC values would be influenced by fixation. For these reasons, we used an indirect approach in this study.

Even though the significance of this study is rather scientific, we believe that any information on tumor behavior and pathophysiology could promote the improvement of therapy that might imply longer survival. It is necessary to know whether diffusion alteration in the normal appearing white matter of glioma patients really indicates tumor infiltration as it has been previously suggested. According to our results, ADC value alone cannot be used as a specific marker of

tumor infiltration in the NAWM of glioma patients, since other factors also seem to alter diffusion as well.

A possible limitation of our study was that different type of structural MPRAGE scans were used to segment the NAWM in the patient and control groups. However, segmented NAWM masks were visually checked and manually corrected on the diffusion images, and these masks were not used for volumetric analysis. Thus it did not influence our results. A further limitation was that we only investigated the role of mass effect among all the possible factors that could lead to ADC elevation in the contralateral NAWM, since tissue samples from the contralateral NAWM were not available. Although steroids might affect diffusion in the brain by decreasing edema, information on steroid treatment was incomplete because of the retrospective design of the study, therefore we were not able to control for steroids in the statistical analysis. Nevertheless, the ADC values we found in the contralateral NAWM were increased and not decreased as we would expect as an effect of steroids.

5.2 Biexponential diffusion alterations in the normal appearing white matter of glioma patients might indicate the presence of global vasogenic edema

Biexponential diffusion analysis enables the detection of subtle changes in tissue microstructure, therefore in this study it was used to gain more precise information about the nature and origin of abnormal diffusion in the NAWM of glioma patients.

Patterns of biexponential parameters can be specific for certain conditions. In cytotoxic edema accompanying acute stroke, the surface area of cell membranes increases due to cell swelling, thus the amount of membrane-bound water rises which results in higher p_{slow} values. The increase of the slow diffusion compartment volume fraction implies the reduction of the fast diffusion component volume fraction that depresses ADC_{mono}, while ADC_{fast} and ADC_{slow} remain relatively unchanged (Brugieres et al., 2004, Le Bihan, 2007, Yoshiura et al., 2010). On the other hand, in vasogenic edema, ADC_{mono}, ADC_{fast} and ADC_{slow} increase, while p_{slow} decreases because of the greater amount of tissue bulk water (Maier et al., 2001, Schwarcz et al., 2007, Maier et al., 2010). In gliomas, higher ADC_{mono} and ADC_{fast} and lower p_{slow} values are present compared to normal

tissues which might be due to altered blood brain barrier permeability and intratumoral edema (Steen, 1992) or to destruction of extracellular matrix structure by tumor infiltration (Morita et al., 2005). ADC_{mono} declines while p_{slow} rises with the increase of cellularity (i.e. tumor grade), since the amount of membrane bound water increases, while ADC_{fast} and ADC_{slow} are not significantly different between low and high grade gliomas (Maier et al., 2001, Le Bihan, 2007, Maier et al., 2010). Table 1, see page 19, summarizes biexponential diffusion parameter changes in different pathologies.

Our results showed elevated ADC_{mono}, ADC_{fast} and ADC_{slow}, and low p_{slow} values in the NAWM of the hemisphere unaffected by the tumor which is similar to the pattern observed in vasogenic edema, cf. Table 1 (Maier et al., 2001). This finding may suggest that edema is present in the normal appearing tissues distant from the tumor. The elevation of ADC_{mono}, ADC_{fast} and ADC_{slow} was present in all regions in the contralateral hemisphere except the temporal NAWM, which indicates that the diffusion abnormality observed in the total hemispheric NAWM does not originate from one region.

Regional differences in diffusion parameters are present in normal white matter (Zhai et al., 2003, Yoshiura et al., 2010). Our results are in agreement with Yoshiura et al. and Zhai et al., who also found the lowest ADC values in the frontal white matter (Zhai et al., 2003, Yoshiura et al., 2010). These regional differences were also present in the contralateral NAWM of glioma patients (shown by the two-way mixed ANOVA analysis). Even though ADC values were higher (and p_{slow} was slightly lower) in all four lobes of the contralateral NAWM of glioma patients, the pattern of regional diffusion differences followed those observed in the NAWM of healthy subjects (i.e. lack of group*region interaction), which indicated that the diffusion abnormality affected the contralateral hemisphere globally. Tumors were not located in the same lobe in all patients which could have also resulted in globally altered diffusion if we hypothesize that diffusion abnormality is caused by tumor infiltration in mirror regions in the contralateral hemisphere. In our study however, the tumors were unevenly distributed between lobes, therefore we believe that the globally altered diffusion is not the result of tumor infiltration, rather it originates from global vasogenic edema.

In the NAWM of the tumor-affected hemisphere, only ADC_{slow} was unchanged compared to controls, whereas the ADC_{mono} and ADC_{fast} were higher and p_{slow} was

lower than control values. This pattern can be observed in gliomas (cf. Table 1), which seems to suggest that tumor infiltration might play a role in diffusion alterations in the NAWM of the ipsilateral hemisphere. The differences of biexponential diffusion parameters between the NAWM of the two hemispheres changed differently in patients and controls (according to the two-way mixed ANOVA analysis). Another possible explanation for the interhemispheric difference of biexponential values is the presence of a greater amount of vasogenic edema in the tumor affected hemisphere.

According to these findings, although infiltrating tumor cells could be present distant from the tumor itself, they seem to contribute more to the diffusion abnormalities in the tumor-affected hemisphere. In contrast with the hypothesis of Ingelese et al. and Kallenberg et al, who explain elevated mean diffusivity in the contralateral NAWM with tumor infiltration (Inglese et al., 2006, Kallenberg et al., 2014), our results seem to suggest this alteration might occur mainly as a result of global vasogenic edema. There might be many factors that could globally alter water diffusion. Although it remains theoretic, these possible factors could be the release of VEGF (Tsai et al., 2003, Toh et al., 2007) or cytokines (Van Meir et al., 1990, Maudsley et al., 2013) implied by the tumor or the alteration of venous drainage (Toh et al., 2007). This theory is further supported by our findings that showed higher ADC values in the NAWM of meningioma patients as well, where VEGF and cytokine secretion is also present (Todo et al., 1994, Nassehi, 2013b), but the lack of tumor infiltration is obvious (DeAngelis, 2001).

A possible limitation of the study is that the glioma group was not homogeneous, with both high grade and low grade glioma patients included. Another limitation might be that the regional NAWM ROIs in the contralateral hemispheres were not created by parcellating the total contralateral hemispheric NAWM ROI, since the software did not make this option possible. Regional ROIs were created and processed separately. Although all ROIs were manually corrected, diffusion values could have been inaccurate in the temporal region due to susceptibility artifacts, which might explain the lack of significant differences between patients and controls in the temporal NAWM. Besides this, possible subtle signal abnormalities in the NAWM close to the peritumoral region might have been undistinguishable from normal tissue on T2-weighted images, which could have caused artificially increased ADC values in the tumor-affected NAWM. Although steroids might affect diffusion in the brain by decreasing edema, patients

receive steroids in a personalized manner, therefore we were not able to control for steroids in the statistical analysis. Nevertheless, the mean ADC values we found in the contralateral NAWM were increased and not decreased as we would expect as an effect of steroids.

5.3 Future perspectives

According to our results, gliomas affect the brain in areas where they are not present. Although this thesis intended to clarify the reason for altered diffusion in NAWM, it is still not clear what exactly happens and how gliomas can induce such abnormalities. This might also raise some questions: are these diffusion abnormalities associated with the poor prognosis of gliomas, and would this alter treatment approach?

The role of tumor infiltration in causing increased ADC in the contralateral NAWM has not been excluded by our results. Although the presence of tumor cell groups was shown by Sahm et al., 2012, we do not think that they could globally alter diffusion in such an extent. Nevertheless, there are several direct and indirect approaches to further investigate the relationship of tumor infiltration in normal tissues with ADC. An indirect approach is the regional analysis of diffusion parameters in patients with identical tumor location (e.g. frontal WM). If ADC is significantly elevated in the WM region contralateral to the tumor compared to other regions, infiltrating glioma cells along the commissural fibers would seem to be the major contributors to increased ADC. The direct relationship of ADC and tumor infiltration could be investigated by correlating ADC values with PET imaging. There are several tracers that appear to be promising in glioma imaging, such as ^{11}C-methionine (Takano et al., 2015), α[(11)C]methyl-L-tryptophan (Jeong et al., 2015), [(18)F]-fluoro-l-thymidine (Collet et al., 2015) , F-fluoroethylcholine (Fraioli et al., 2015).

We believe that diffusion alterations in the NAWM occur as a result of a global compensation mechanism which is a response to the presence of the tumor. This might happen due to the failure of venous drainage produced by tumor compression or due to altered water balance in the brain. Although ADC values did not show any relationship to tumor volumes, other characteristics of tumor size, growth rate or intracranial pressure might correlate with diffusion parameters. Global vasogenic edema might be related to altered aquaporin channel status,

VEGF secretion or cytokine secretion. The alteration of these factors could be investigated in post-mortem glioma-affected brains. The association of cytokine secretion and altered ADC could be investigated by measuring ADC values in non- demyelinizating neuroinflammatory brain diseases (the loss of myelin leads to altered ADC (Nagy et al., 2013b)). Although it remains hypothetic, genetic factors might also play a role in altered diffusion.

Although our results have more scientific value than clinical, our findings might possibly be clinically useful in the future. If the observed global diffusion abnormality was related to tumor growth rate or malignancy, prognosis could be assessed from a single time point scan instead of using a series of control scans.

6. Summary

Altered diffusion in the NAWM of glioma patients has previously been explained by tumor infiltration. In this thesis we intended to clarify the nature of elevated ADC in the NAWM of glioma patients.

Our study tested the hypothesis whether abnormal ADC values in the normal appearing white matter contralateral to brain tumors can be explained exclusively by tumor infiltration.

An indirect way to test this hypothesis was to check if ADC was altered in the contralateral NAWM of patients with non-infiltrative tumors. We assumed, if ADC was increased in the NAWM of both infiltrative tumor (i.e. glioma) and non-infiltrative tumor (i.e. meningioma) patients, the diffusion alteration could not had been explained exclusively by the presence of tumor infiltration.

Our results revealed elevated ADC in the contralateral NAWM of both infiltrative and non-infiltrative tumor patients that might suggest that the effect of infiltrating tumor cells is not the only reason for the alteration. One alternative explanation, mass effect, was investigated and not found to play a role in increasing ADC values in the contralateral NAWM, since ADC in the contralateral NAWM was not related to tumor volume.

The literature was searched for other possible factors that could explain our results. There are complex mechanisms that might be present in both infiltrative and non-infiltrative tumors possible related to the secretory activity of the tumors. Besides these, effects of tumor infiltration in infiltrative tumors might also contribute to elevated ADC. This contribution seems to be greater in the NAWM of high grade glioma patients than in low grade glioma patients.

In the second study, we aimed to reveal the cause of observed diffusion abnormality prospectively with the slow (structured) and fast (free) diffusing water compartment model described by LeBihan. The biexponential analysis revealed increased ADC_{mono}, ADC_{fast} and ADC_{slow} values and decreased p_{slow} value in the NAWM of the unaffected hemisphere of glioma patients, which suggested the presence of global vasogenic brain edema in glioma patients. This study revealed that regional differences in patients followed those found in controls, which also supported the global nature of the phenomenon. Besides the presence of edema, tumor infiltration might be responsible for the diffusion abnormalities in the

ipsilateral NAWM, however, the increase in ADC is probably not an indicator of tumor infiltration only.

In conclusion, our retrospective study including non-infiltrative and infiltrative patients showed, that altered diffusion in the NAWM is not exclusively caused by tumor infiltration, although the difference between low and high grade gliomas might indicate some degree of infiltration. One alternative explanation, mass effect was excluded during the first study. The potential role of vasogenic edema in causing the observed diffusion alterations was shown in the second, prospective study. Our results might contribute to the development of diagnostic or prognostic methods in the future.

7. References

Assaf Y, Cohen Y (1998a) In vivo and in vitro bi-exponential diffusion of N-acetyl aspartate (NAA) in rat brain: a potential structural probe? NMR in Biomedicine 11:67-74.

Assaf Y, Cohen Y (1998b) Non-mono-exponential attenuation of water and N-acetyl aspartate signals due to diffusion in brain tissue. Journal of Magnetic Resonance 131:69-85.

Assaf Y, Cohen Y (2000) Assignment of the water slow-diffusing component in the central nervous system using q-space diffusion MRS: implications for fiber tract imaging. Magnetic Resonance in Medicine 43:191-199.

Assaf Y, Freidlin RZ, Rohde GK, Basser PJ (2004) New modeling and experimental framework to characterize hindered and restricted water diffusion in brain white matter. Magnetic Resonance in Medicine 52:965-978.

Bashir R, Hochberg F, Oot R (1988) Regrowth patterns of glioblastoma multiforme related to planning of interstitial brachytherapy radiation fields. Neurosurgery 23:27-30.

Batchelor TT, Sorensen AG, di Tomaso E, Zhang WT, Duda DG, Cohen KS, Kozak KR, Cahill DP, Chen PJ, Zhu M, Ancukiewicz M, Mrugala MM, Plotkin S, Drappatz J, Louis DN, Ivy P, Scadden DT, Benner T, Loeffler JS, Wen PY, Jain RK (2007) AZD2171, a pan-VEGF receptor tyrosine kinase inhibitor, normalizes tumor vasculature and alleviates edema in glioblastoma patients. Cancer Cell 11:83-95.

Bennett KM, Schmainda KM, Bennett RT, Rowe DB, Lu H, Hyde JS (2003) Characterization of continuously distributed cortical water diffusion rates with a stretched-exponential model. Magnetic Resonance in Medicine 50:727-734.

Bieza A, Krumina G (2012) Magnetic resonance study on fractional anisotropy and neuronal metabolite ratios in peritumoral area of cerebral gliomas. Medicina (Kaunas) 48:497-506.

Black KL, Chen K, Becker DP, Merrill JE (1992) Inflammatory leukocytes associated with increased immunosuppression by glioblastoma. Journal of Neurosurgery 77:120-126.

Brugieres P, Thomas P, Maraval A, Hosseini H, Combes C, Chafiq A, Ruel L, Breil S, Peschanski M, Gaston A (2004) Water diffusion compartmentation at high b values in ischemic human brain. American Journal of Neuroradiology 25:692-698.

Bulakbasi N, Guvenc I, Onguru O, Erdogan E, Tayfun C, Ucoz T (2004) The added value of the apparent diffusion coefficient calculation to magnetic resonance imaging in the differentiation and grading of malignant brain tumors. Journal of Computer Assisted Tomography 28:735-746.

Cha S (2006) Update on brain tumor imaging: from anatomy to physiology. American Journal of Neuroradiology 27:475-487.

Chan YH (2004) Biostatistics 201: linear regression analysis. Singapore Medical Journal 45:55-61.

Chen KC, Nicholson C (2000) Changes in brain cell shape create residual extracellular space volume and explain tortuosity behavior during osmotic challenge. Proceedings of the National Academy of Sciences of the United States of America 97:8306-8311.

Cohen BA, Knopp EA, Rusinek H, Babb JS, Zagzag D, Gonen O (2005) Assessing global invasion of newly diagnosed glial tumors with whole-brain proton MR spectroscopy. American Journal of Neuroradiology 26:2170-2177.

Collet S, Valable S, Constans JM, Lechapt-Zalcman E, Roussel S, Delcroix N, Abbas A, Ibazizene M, Bernaudin M, Barre L, Derlon JM, Guillamo JS (2015) [(18)F]-fluoro-L-thymidine PET and advanced MRI for preoperative grading of gliomas. NeuroImage Clinical 8:448-454.

Collins DL, Neelin P, Peters TM, Evans AC (1994) Automatic 3D intersubject registration of MR volumetric data in standardized Talairach space. Journal of Computer Assisted Tomography 18:192-205.

DeAngelis LM (2001) Brain tumors. The New England journal of medicine 344:114-123.

Ebisu T, Naruse S, Horikawa Y, Ueda S, Tanaka C, Uto M, Umeda M, Higuchi T (1993) Discrimination between different types of white matter edema with diffusion-weighted MR imaging. Journal of Magnetic Resonance Imaging 3:863-868.

Essig M, Anzalone N, Combs SE, Dorfler A, Lee SK, Picozzi P, Rovira A, Weller M, Law M (2012) MR imaging of neoplastic central nervous system lesions: review and recommendations for current practice. American Journal of Neuroradiology 33:803-817.

Essig M, Nguyen TB, Shiroishi MS, Saake M, Provenzale JM, Enterline DS, Anzalone N, Dorfler A, Rovira A, Wintermark M, Law M (2013) Perfusion MRI: the five most frequently asked clinical questions. American Journal of Roentgenology 201:W495-510.

Essig M, Schlemmer HP, Tronnier V, Hawighorst H, Wirtz R, van Kaick G (2001) Fluid-attenuated inversion-recovery MR imaging of gliomatosis cerebri. European Radiology 11:303-308.

Fedorov A, Beichel R, Kalpathy-Cramer J, Finet J, Fillion-Robin JC, Pujol S, Bauer C, Jennings D, Fennessy F, Sonka M, Buatti J, Aylward S, Miller JV, Pieper S, Kikinis R (2012) 3D Slicer as an image computing platform for the Quantitative Imaging Network. Magnetic Resonance Imaging 30:1323-1341.

Fischl B, Salat DH, Busa E, Albert M, Dieterich M, Haselgrove C, van der Kouwe A, Killiany R, Kennedy D, Klaveness S, Montillo A, Makris N, Rosen B, Dale AM (2002) Whole brain segmentation: automated labeling of neuroanatomical structures in the human brain. Neuron 33:341-355.

Fischl B, Salat DH, van der Kouwe AJ, Makris N, Segonne F, Quinn BT, Dale AM (2004) Sequence-independent segmentation of magnetic resonance images. NeuroImage 23 Suppl 1:S69-84.

Fischl B, Sereno MI, Dale AM (1999) Cortical surface-based analysis. II: Inflation, flattening, and a surface-based coordinate system. NeuroImage 9:195-207.

Folkman J (1990) What is the evidence that tumors are angiogenesis dependent? Journal of the National Cancer Institute 82:4-6.

Fraioli F, Shankar A, Hargrave D, Hyare H, Gaze MN, Groves AM, Alongi P, Stoneham S, Michopoulou S, Syed R, Bomanji JB (2015) 18F-fluoroethylcholine (18F-Cho) PET/MRI functional parameters in pediatric astrocytic brain tumors. Clinical Nuclear Medicine 40:e40-45.

Giese A, Bjerkvig R, Berens ME, Westphal M (2003) Cost of migration: invasion of malignant gliomas and implications for treatment. Journal of Clinical Oncology 21:1624-1636.

Giese A, Loo MA, Tran N, Haskett D, Coons SW, Berens ME (1996) Dichotomy of astrocytoma migration and proliferation. International Journal of Cancer 67:275-282.

Hazlewood CF, Rorschach HE, Lin C (1991) Diffusion of water in tissues and MRI. Magnetic Resonance in Medicine 19:214-216.

Helenius J, Soinne L, Perkio J, Salonen O, Kangasmaki A, Kaste M, Carano RA, Aronen HJ, Tatlisumak T (2002) Diffusion-weighted MR imaging in normal human brains in various age groups. American Journal of Neuroradiology 23:194-199.

Inglese M, Brown S, Johnson G, Law M, Knopp E, Gonen O (2006) Whole-brain N-acetylaspartate spectroscopy and diffusion tensor imaging in patients with newly diagnosed gliomas: a preliminary study. American Journal of Neuroradiology 27:2137-2140.

Jenkinson M, Bannister P, Brady M, Smith S (2002) Improved optimization for the robust and accurate linear registration and motion correction of brain images. NeuroImage 17:825-841.

Jensen JH, Helpern JA (2010) Progress in diffusion-weighted imaging: concepts, techniques and applications to the central nervous system. NMR in Biomedicine 23:659-660.

Jensen JH, Helpern JA, Ramani A, Lu H, Kaczynski K (2005) Diffusional kurtosis imaging: the quantification of non-gaussian water diffusion by means of magnetic resonance imaging. Magnetic Resonance in Medicine 53:1432-1440.

Jeong JW, Juhasz C, Mittal S, Bosnyak E, Kamson DO, Barger GR, Robinette NL, Kupsky WJ, Chugani DC (2015) Multi-modal imaging of tumor cellularity and Tryptophan metabolism in human Gliomas. Cancer Imaging 15:10.

Johansen-Berg H (2009) Imaging the relationship between structure, function and behaviour in the human brain. Brain Structure & Function 213:499-500.

Kallenberg K, Goldmann T, Menke J, Strik H, Bock HC, Mohr A, Buhk JH, Frahm J, Dechent P, Knauth M (2014) Abnormalities in the normal appearing white matter of the cerebral hemisphere contralateral to a malignant brain tumor detected by diffusion tensor imaging. Folia Neuropathologica 52:226-233.

Kallenberg K, Goldmann T, Menke J, Strik H, Bock HC, Stockhammer F, Buhk JH, Frahm J, Dechent P, Knauth M (2013) Glioma infiltration of the corpus callosum: early signs detected by DTI. Journal of Neuro-Oncology 112:217-222.

Kiselev VG, Il'yasov KA (2007) Is the "biexponential diffusion" biexponential? Magnetic Resonance in Medicine 57:464-469.

Kitis O, Altay H, Calli C, Yunten N, Akalin T, Yurtseven T (2005) Minimum apparent diffusion coefficients in the evaluation of brain tumors. European Journal of Radiology 55:393-400.

Klimas A, Drzazga Z, Kluczewska E, Hartel M (2013) Regional ADC measurements during normal brain aging in the clinical range of b values: a DWI study. Clinical Imaging 37:637-644.

Larsen VA, Simonsen HJ, Law I, Larsson HB, Hansen AE (2013) Evaluation of dynamic contrast-enhanced T1-weighted perfusion MRI in the differentiation of tumor recurrence from radiation necrosis. Neuroradiology 55:361-369.

Law M, Yang S, Wang H, Babb JS, Johnson G, Cha S, Knopp EA, Zagzag D (2003) Glioma grading: sensitivity, specificity, and predictive values of perfusion MR imaging and proton MR spectroscopic imaging compared with conventional MR imaging. American Journal of Neuroradiology 24:1989-1998.

Le Bihan D (1995) Molecular diffusion, tissue microdynamics and microstructure. NMR in Biomedicine 8:375-386.

Le Bihan D (2007) The 'wet mind': water and functional neuroimaging. Physics in Medicine and Biology 52:R57-90.

Le Bihan D (2013) Apparent diffusion coefficient and beyond: what diffusion MR imaging can tell us about tissue structure. Radiology 268:318-322.

Le Bihan D, Breton E, Lallemand D, Grenier P, Cabanis E, Laval-Jeantet M (1986) MR imaging of intravoxel incoherent motions: application to diffusion and perfusion in neurologic disorders. Radiology 161:401-407.

Le Bihan D, Johansen-Berg H (2012) Diffusion MRI at 25: exploring brain tissue structure and function. NeuroImage 61:324-341.

Louis DN, Ohgaki H, Wiestler OD, Cavenee WK, Burger PC, Jouvet A, Scheithauer BW, Kleihues P (2007) The 2007 WHO classification of tumours of the central nervous system. Acta Neuropathologica 114:97-109.

Louis DN, Perry A, Burger P, Ellison DW, Reifenberger G, von Deimling A, Aldape K, Brat D, Collins VP, Eberhart C, Figarella-Branger D, Fuller GN, Giangaspero F, Giannini C, Hawkins C, Kleihues P, Korshunov A, Kros JM, Beatriz Lopes M, Ng HK, Ohgaki H, Paulus W, Pietsch T, Rosenblum M, Rushing E, Soylemezoglu F, Wiestler O, Wesseling P (2014) International Society Of Neuropathology--Haarlem consensus guidelines for nervous system tumor classification and grading. Brain Pathology 24:429-435.

Lu S, Ahn D, Johnson G, Cha S (2003) Peritumoral diffusion tensor imaging of high-grade gliomas and metastatic brain tumors. American Journal of Neuroradiology 24:937-941.

Ma C, Zhao G, Cruz MH, Siden A, Yakisich JS (2014) Translational gap in glioma research. Anti-Cancer Agents in Medical Chemistry 14:1110-1120.

Maier SE, Bogner P, Bajzik G, Mamata H, Mamata Y, Repa I, Jolesz FA, Mulkern RV (2001) Normal brain and brain tumor: multicomponent apparent diffusion coefficient line scan imaging. Radiology 219:842-849.

Maier SE, Gudbjartsson H, Patz S, Hsu L, Lovblad KO, Edelman RR, Warach S, Jolesz FA (1998) Line scan diffusion imaging: characterization in healthy subjects and stroke patients. American Journal of Roentgenology 171:85-93.

Maier SE, Mulkern RV (2008) Biexponential analysis of diffusion-related signal decay in normal human cortical and deep gray matter. Magnetic Resonance Imaging 26:897-904.

Maier SE, Sun Y, Mulkern RV (2010) Diffusion imaging of brain tumors. NMR in Biomedicine 23:849-864.

Maudsley AA, Roy B, Gupta RK, Sheriff S, Awasthi R, Gu M, Husain N, Mohakud S, Behari S, Spielman DM (2013) Association of Metabolite Concentrations and Water Diffusivity in Normal Appearing Brain Tissue with Glioma Grade. Journal of Neuroimaging 24(6):585-9

Mayhan WG (1999) VEGF increases permeability of the blood-brain barrier via a nitric oxide synthase/cGMP-dependent pathway. American Journal of Physiology - Cell Physiology 276:C1148-C1153.

Mikkelsen T, Yan PS, Ho KL, Sameni M, Sloane BF, Rosenblum ML (1995) Immunolocalization of cathepsin B in human glioma: implications for tumor invasion and angiogenesis. Journal of Neurosurgery 83:285-290.

Moffat BA, Chenevert TL, Lawrence TS, Meyer CR, Johnson TD, Dong Q, Tsien C, Mukherji S, Quint DJ, Gebarski SS, Robertson PL, Junck LR, Rehemtulla A, Ross BD (2005) Functional diffusion map: a noninvasive MRI biomarker for early stratification of clinical brain tumor response. Proceedings of the National Academy of Sciences of the United States of America 102:5524-5529.

Morita K, Matsuzawa H, Fujii Y, Tanaka R, Kwee IL, Nakada T (2005) Diffusion tensor analysis of peritumoral edema using lambda chart analysis indicative of the heterogeneity of the microstructure within edema. Journal of Neurosurgery 102:336-341.

Mulkern RV, Haker SJ, Maier SE (2009) On high b diffusion imaging in the human brain: ruminations and experimental insights. Magnetic resonance imaging 27:1151-1162.

Naganawa S, Sato K, Katagiri T, Mimura T, Ishigaki T (2003) Regional ADC values of the normal brain: differences due to age, gender, and laterality. European Radiology 13:6-11.

Nagy SA, Aradi M, Orsi G, Perlaki G, Kamson DO, Mike A, Komaromy H, Schwarcz A, Kovacs A, Janszky J, Pfund Z, Illes Z, Bogner P (2013a) Bi-exponential diffusion signal decay in normal appearing white matter of multiple sclerosis. Magnetic Resonance Imaging 31:286-295.

Nagy SA HR, Perlaki G, Orsi G, Barsi P, John F, Horvath A, Kovacs N, Bogner P, Janszky J (2016) Age at onset and seizure frequency affect white matter diffusion coefficient in patients with mesial temporal lobe epilepsy. Epilepsy & Behavior (submitted).

Nassehi D (2013a) Intracranial meningiomas, the VEGF-A pathway, and peritumoral brain oedema. Danish Medical Journal 60:B4626.

Nicholson C, Sykova E (1998) Extracellular space structure revealed by diffusion analysis. Trends in Neurosciences 21:207-215.

Niendorf T, Dijkhuizen RM, Norris DG, van Lookeren Campagne M, Nicolay K (1996) Biexponential diffusion attenuation in various states of brain tissue: implications for diffusion-weighted imaging. Magnetic Resonance in Medicine 36:847-857.

Olson JJ, Nayak L, Ormond DR, Wen PY, Kalkanis SN, Ryken TC (2014) The role of targeted therapies in the management of progressive glioblastoma : a systematic review and evidence-based clinical practice guideline. Journal of Neuro-Oncology 118:557-599.

Orsi G, Aradi M, Nagy SA, Perlaki G, Trauninger A, Bogner P, Janszky J, Illés Z, Dóczi T, Pfund Z, Schwarcz A (2015) Differentiating white matter lesions in multiple sclerosis and migraine using monoexponential and biexponential diffusion measurements. Journal of Magnetic Resonance Imaging 41(3):676-83

Ostrom QT, Gittleman H, Fulop J, Liu M, Blanda R, Kromer C, Wolinsky Y, Kruchko C, Barnholtz-Sloan JS (2015) CBTRUS Statistical Report: Primary Brain and Central Nervous System Tumors Diagnosed in the United States in 2008-2012. Neuro-Oncology 17 Suppl 4:iv1-iv62.

Pauleit D, Langen KJ, Floeth F, Hautzel H, Riemenschneider MJ, Reifenberger G, Shah NJ, Muller HW (2004) Can the apparent diffusion coefficient be used as a noninvasive parameter to distinguish tumor tissue from peritumoral tissue in cerebral gliomas? Journal of Magnetic Resonance Imaging 20:758-764.

Plate KH, Breier G, Weich HA, Risau W (1992) Vascular endothelial growth factor is a potential tumour angiogenesis factor in human gliomas in vivo. Nature 359:845-848.

Provenzale JM, McGraw P, Mhatre P, Guo AC, Delong D (2004) Peritumoral brain regions in gliomas and meningiomas: investigation with isotropic diffusion-weighted MR imaging and diffusion-tensor MR imaging. Radiology 232:451-460.

Puttick S, Bell C, Dowson N, Rose S, Fay M PET, MRI, and simultaneous PET/MRI in the development of diagnostic and therapeutic strategies for glioma: Drug Discovery Today. 2014 S1359-6446(14)00421-8.

Rochfort KD, Cummins PM (2015) The blood-brain barrier endothelium: a target for pro-inflammatory cytokines. Biochemical Society Transactions 43:702-706.

Romano A, Fasoli F, Ferrante M, Ferrante L, Fantozzi LM, Bozzao A (2008) Fiber density index, fractional anisotropy, adc and clinical motor findings in the white matter of patients with glioblastoma. European Radiology 18:331-336.

Rowley HA, Grant PE, Roberts TP (1999) Diffusion MR imaging. Theory and applications. Neuroimaging Clinics of North America 9:343-361.

Roy B, Gupta RK, Maudsley AA, Awasthi R, Sheriff S, Gu M, Husain N, Mohakud S, Behari S, Pandey CM, Rathore RK, Spielman DM, Alger JR (2013) Utility of multiparametric 3-T MRI for glioma characterization. Neuroradiology 55:603-613.

Runge VM, Kirsch JE, Burke VJ, Price AC, Nelson KL, Thomas GS, Dean BL, Lee C (1992) High-dose gadoteridol in MR imaging of intracranial neoplasms. Journal of Magnetic Resonance Imaging 2:9-18.

Sahm F, Capper D, Jeibmann A, Habel A, Paulus W, Troost D, von Deimling A (2012) Addressing diffuse glioma as a systemic brain disease with single-cell analysis. Archives of Neurology 69:523-526.

Schwarcz A, Ursprung Z, Berente Z, Bogner P, Kotek G, Meric P, Gillet B, Beloeil JC, Doczi T (2007) In vivo brain edema classification: New insight offered by large b-value diffusion-weighted MR imaging. Journal of Magnetic Resonance Imaging 25:26-31.

Segonne F, Dale AM, Busa E, Glessner M, Salat D, Hahn HK, Fischl B (2004) A hybrid approach to the skull stripping problem in MRI. NeuroImage 22:1060-1075.

Siegal T (2015) Clinical impact of molecular biomarkers in gliomas. Journal of Clinical Neuroscience 22:437-444.

Sotak CH (2004) Nuclear magnetic resonance (NMR) measurement of the apparent diffusion coefficient (ADC) of tissue water and its relationship to

cell volume changes in pathological states. Neurochemistry International 45:569-582.

Stanisz GJ, Szafer A, Wright GA, Henkelman RM (1997) An analytical model of restricted diffusion in bovine optic nerve. Magnetic Resonance in Medicine 37:103-111.

Steen RG (1992) Edema and tumor perfusion: characterization by quantitative 1H MR imaging. American Journal of Roentgenology 158:259-264.

Stejskal EO, Tanner JE (1965) Spin Diffusion Measurements: Spin Echoes in the Presence of a Time-Dependent Field Gradient. The Journal of Chemical Physics 42:288-292.

Stupp R, Roila F (2009) Malignant glioma: ESMO clinical recommendations for diagnosis, treatment and follow-up. Annals of Oncology ESMO 20 Suppl 4:126-128.

Sugahara T, Korogi Y, Kochi M, Ikushima I, Shigematu Y, Hirai T, Okuda T, Liang L, Ge Y, Komohara Y, Ushio Y, Takahashi M (1999) Usefulness of diffusion-weighted MRI with echo-planar technique in the evaluation of cellularity in gliomas. Journal of Magnetic Resonance Imaging 9:53-60.

Takano K, Kinoshita M, Arita H, Okita Y, Chiba Y, Kagawa N, Fujimoto Y, Kishima H, Kanemura Y, Nonaka M, Nakajima S, Shimosegawa E, Hatazawa J, Hashimoto N, Yoshimine T (2015) Diagnostic and Prognostic Value of 11C-Methionine PET for Nonenhancing Gliomas. American Journal of Neuroradiology.

Thoeny HC, Ross BD. (2010) Predicting and Monitoring Cancer Treatment Response with DW-MRI. Journal of Magnetic Resonance Imaging 32(1), 2–16.

Todo T, Adams EF, Rafferty B, Fahlbusch R, Dingermann T, Werner H (1994) Secretion of interleukin-6 by human meningioma cells: possible autocrine inhibitory regulation of neoplastic cell growth. Journal of Neurosurgery 81:394-401.

Toh CH, Wong AM, Wei KC, Ng SH, Wong HF, Wan YL (2007) Peritumoral edema of meningiomas and metastatic brain tumors: differences in diffusion characteristics evaluated with diffusion-tensor MR imaging. Neuroradiology 49:489-494.

Tsai JC, Teng LJ, Chen CT, Hong TM, Goldman CK, Gillespie GY (2003) Protein kinase C mediates induced secretion of vascular endothelial growth factor by human glioma cells. Biochemical and Biophysical Research Communications 309:952-960.

Van Meir E, Sawamura Y, Diserens AC, Hamou MF, de Tribolet N (1990) Human glioblastoma cells release interleukin 6 in vivo and in vitro. Cancer Research 50:6683-6688.

Wedeen VJ, Hagmann P, Tseng WY, Reese TG, Weisskoff RM (2005) Mapping complex tissue architecture with diffusion spectrum magnetic resonance imaging. Magnetic Resonance in Medicine 54:1377-1386.

Wieshmann UC, Symms MR, Parker GJ, Clark CA, Lemieux L, Barker GJ, Shorvon SD (2000) Diffusion tensor imaging demonstrates deviation of fibres in normal appearing white matter adjacent to a brain tumour. Journal of Neurology, Neurosurgery, and Psychiatry 68:501-503.

Yablonskiy DA, Bretthorst GL, Ackerman JJ (2003) Statistical model for diffusion attenuated MR signal. Magnetic Resonance in Medicine 50:664-669.

Yoshiura T, Noguchi T, Hiwatashi A, Togao O, Yamashita K, Nagao E, Kamano H, Honda H (2010) Intra- and interhemispheric variations of diffusivity in subcortical white matter in normal human brain. European Radiology 20:227-233.

Zhai G, Lin W, Wilber KP, Gerig G, Gilmore JH (2003) Comparisons of regional white matter diffusion in healthy neonates and adults performed with a 3.0-T head-only MR imaging unit. Radiology 229:673-681.

8. List of publications

8.1. Articles related to this thesis

Horvath A, Perlaki G, Toth A, Orsi G, Nagy S, Doczi T, Horvath Z, Bogner P (2016) Increased diffusion in the normal appearing white matter of brain tumor patients: is this just tumor infiltration? Journal of Neuro-Oncology 127(1):83-90. IF: **3.070** (in 2014)

Horvath A, Perlaki G, Toth A, Orsi G, Nagy S, Doczi T, Horvath Z, Bogner P (2016) Biexponential diffusion alterations in the normal-appearing white matter of glioma patients might indicate the presence of global vasogenic edema. Journal of Magnetic Resonance Imaging (Epud ahead of print). **IF: 3.21** (in 2014)

8.2 Articles unrelated to this thesis

Horváth A, Nagy SA, Perlaki G, Orsi G, Bogner P, Dóczi T (2015) Multimodal Quantitative Characterization of Intracranial Epidermoid Cysts: Preliminary Results. Ideggyogyaszati szemle 68:347-355. **IF: 0.386** (in 2014)

Toth A, Kovacs N, Tamas V, Kornyei B, Nagy M, **Horvath A**, Rostas T, Bogner P, Janszky J, Doczi T, Buki A, Schwarcz A (2016) Microbleeds may expand acutely after traumatic brain injury. Neuroscience Letters 617:207-12. **IF: 2.030** (in 2014)

Nagy SA HR, Perlaki G, Orsi G, Barsi P, John F, **Horvath A,** Kovacs N, Bogner P, Janszky J (2016) Age at onset and seizure frequency affect white matter diffusion coefficient in patients with mesial temporal lobe epilepsy. Epilepsy & Behavior (submitted).

Aschermann Z, Perlaki G, Orsi G, Nagy SA, **Horvath A**, Bone B, Bihari K, Acs P, Janszky J, Komoly S, Bogner P (2015) Quantitative assessment of brain iron by R2* relaxometry in patients with cervical dystonia. Movement disorders : official journal of the Movement Disorder Society 30:1422-1426. **IF: 5.68** (in 2014)

Kellermayer MS, Murvai U, **Horvath A**, Laszloffi E, Soos K, Penke B (2013) Epitaxial assembly dynamics of mutant amyloid beta25-35_N27C fibrils explored with time-resolved scanning force microscopy. Biophysical chemistry 184:54-61. **IF: 2.319**

Horváth A, Aradi M, Perlaki G, Orsi G, Szalay Cs, Schwarcz A, Büki A, Kövér F, Dóczi T, Bogner P (2013) A kómás agy strukturális és funkcionális vizsgálata multiparametrikus MR technikával. Magyar Radiológia 87(2):32-39

8.3 Presentations related to this thesis

Horváth A, Perlaki G, Toth A, Orsi G, Nagy S, Doczi T, Horvath Z, Bogner P. *Comparison of diffusion alterations in the normal appearing white matter of glioma and meningioma patients*. 47th Annual Meeting HMAA – Current Developments in Biomedical and Clinical Sciences, Sarasota, FL, United States of America, 2015.

Horváth A, Perlaki G, Toth A, Orsi G, Nagy S, Doczi T, Horvath Z, Bogner P. *Comparison of diffusion alterations in the normal appearing white matter of glioma and meningioma patients*. 53rd American Society of Neuroradiology Annual Meeting, Chicago, IL, United States of America, 2015

Horváth A, Perlaki G, Toth A, Orsi G, Nagy S, Doczi T, Horvath Z, Bogner P. *Tumor infiltration cannot be the only reason for diffusion alerations in the normal apperaing white matter in brain tumors*. HMAA Conference in Balatonfüred 2015.

Horváth A, Perlaki G, Tóth A, Orsi G, Nagy S, Dóczi T, Horváth Z, Bogner P. *Diffusion alterations in the normal appearing white matter of glioma and meningioma patients*. Neuroimaging Workshop, Szeged, 2015.

Horváth A., Nagy SA, Perlaki G, Orsi G, Tóth A, Dóczi T, Horváth Zs, Bogner P. *Megváltozott szöveti diffúzió gliómás betegek épnek tűnő fehérállományában.* Neuroscience Centre /Szentágothai Research Centre PhD and Medical Student Congress, 2014.

Horváth A., Nagy SA, Perlaki G, Orsi G, Tóth A, Dóczi T, Horváth Zs, Bogner P. *Megváltozott szöveti diffúzió gliómás betegek épnek tűnő fehérállományában.* 22nd Annual Meeting of the Hungarian Society of Neuroradiology. Hajdúszoboszló, 2014.

8.4. Presentations unrelated to this thesis

Horváth A, Várallyay C, Várallyay P, Schwartz D, Ambady P, Bogner P, Neuwelt E. *Comparison of ferumoxytol and gadolinium enhancement changes in response to Avastin in high grade glioma patients.* International Society for Magnetic Resonance in Medicine 24th Annual Meeting, Singapore, 2016

Horváth A, Várallyay C, Szidonya L, Várallyay P, Schwartz D, Ambady P, Bogner P, Neuwelt E. *Comparison of gadolinium and ferumoxytol enhancement in treated glioma patients: preliminary results*. Radiology Research Retreat, Portland, OR, United States of America, 2016

Horváth A, Várallyay C, Várallyay P, Schwartz D, Ambady P, Bogner P, Neuwelt E. *Comparison of ferumoxytol and gadolinium enhancement changes in response to Avastin in high grade glioma patients.* European Congress of Radiology, Vienna, Austria, 2016

Horváth A, Várallyay C, Várallyay P, Schwartz D, Ambady P, Bogner P, Neuwelt E. *Comparison of gadolinium and ferumoxytol enhancement in treated glioma pateints: preliminary results*. 23rd Annual Meeting of the Hungarian Society of Neuroradiology, 2014.

Péter Horváth, **Horváth A**, Péter Bogner, Zsolt Horváth. *The evaluation of cerebral atrophy after whole brain radiation therapy with MRI volumetry*. Grastyán Congress, 2015

Várallyay, C, **Horváth A**, Neuwelt, E. Ferumoxytol as an MRI Contrast agent in th CNS; Collaborations and multicenter trials.. 47th Annual Meeting HMAA – Current Developments in Biomedical and Clinical Sciences, Sarasota, FL, United States of America, 2015.

Orsi G, Perlaki G, Horváth R, Nagy SA, **Horváth A**, Bogner P, Janszky J. *Comparison of accuracz between FSL's FIRST and Freesurfer for caudate nucleus and putamen segmentation.* Magnatic resonance Materials in Physics and Biology and Medicine. ESMRMB Congress, Edinburgh, United Kingdom 2015.

Horváth P, **Horváth A**, Bogner P, Horváth Z. *The evaluation of cerebral atrophy after whole brain radiation therapy with MRI volumetry*. HMAA Conference in Balatonfüred 2015.

Környei B., **Horváth A**, Tóth A. *Follow-up susceptibility weighted (SWI) MRI study on traumatic brain injuries (TBI): revealing the leasions' dinamics*. HMAA Conference in Balatonfüred 2015.

Herczeg B, **Horváth A**, Horváth Z, Bogner P, Vető F. *Kinél segít a shunt? Liquortér volumetria hydrocephalusos betegekben*. HMAA Conference in Balatonfüred 2015.

Toth A, Kovacs N, Tamas V, Kornyei B, Nagy M, **Horvath A**, Bogner P, Janszky J, Doczi T, Buki A, Schwarcz A. *Microbleeds may progress acutely after traumatic brain injury*. Neuroimaging Workshop, Szeged, 2015

Orsi G, Perlaki G, Horvath R, Nagy SA, **Horváth A**, Bogner P, Janszky J. *Comparison of accuracy between FSL's FIRST and Freesurfer for caudate nucleus and putamen segmentation*. Neuroimaging Workshop, Szeged, 2015

Nagy SA, Horváth R, John F, Janszky J, Perlaki G, **Horváth A**, Bogner P. *Legújabb MR módszerek és alkalmazási területeik különböző intracraniális betegségekben.* X. Jubileumi Képalkotó Diagnosztikai Továbbképzés és Konferencia, Budapest, 2015.

Horváth A, Nagy SA, Perlaki G, Orsi G, Tóth A, Dóczi T, Bogner P.Multimodal quantitative characterization of intracranial epidermoid cysts: preliminary results. HMAA Conference in Balatonfüred 2014.

Horváth A., Nagy SA, Perlaki G, Orsi G, Tóth A, Horváth Zs, Dóczi T, Bogner P. New Trends in Perfusion MR Imaging. Neuroimaging Workshop, Debrecen, 2014.

Horváth A, Nagy SA, Perlaki G, Orsi G, Aradi M, Horváth Z, Dóczi T, Bogner P*. Perfúziós MR vizsgálati metodikák összehasonlítása cerebrális neoplazmákban.* 21st Annual Meeting of the Hungarian Society of Neuroradiology. Visegrád, 2013.

Horváth A, Aradi M, Perlaki G, Orsi G, Tóth A, Schwarcz A, Büki A, Kövér F, Dóczi T, Bogner P*. Kómás betegek kognitív funkcióinak vizsgálata funkcionális MR, diffúzió tenzor képalkotással és ^{1}H- spektroszkópiával.* National Student Research Conference, Szeged, 2013.

Horváth A, Aradi M, Perlaki G, Orsi G, Tóth A, Schwarcz A, Büki A, Kövér F, Dóczi T, Bogner*. Kómás betegek kognitív funkcióinak vizsgálata funkcionális MR, diffúzió tenzor képalkotással és ^{1}H- spektroszkópiával.* Student Research Conference, Pécs, 2013.

Horváth A, Aradi M, Perlaki G, Orsi G, Tóth A, Schwarcz A, Büki A, Kövér F, Dóczi T, Bogner P *. The evaluation of comatose brain with fMRI, DTI and 1H – spectroscopy.* 44. Annual Meeting HMAA – Current Developments in Biomedical and Clinical Sciences, Sarasota, FL, United States of America, 2012.

Horváth A, Nagy S, Aradi M, Orsi G, Perlaki G, Komáromy H, Schwarcz A, Janszky J, Bogner P*. Quantitative MR imaging of cholesteatoma with T1 and T2 mapping.* HMAA Conference in Balatonfüred 2012.

Horváth A, Nagy SA, Dóczi T, Bogner P*. A cholesteatoma kvantitatív MR vizsgálata, avagy a T2 térképezés módszere.* Student Research Conference, Pécs. 2012.

Horváth A, Aradi M, Perlaki G, Orsi G, Schwarcz A, Büki A, Kövér F, Dóczi T, Bogner P*. The evaluation of comatose brain with fMRI, DTI and 1H – spectroscopy.* HMAA Conference in Balatonfüred 2011.

Kellermeyer MSZ, **Horváth A**, Murvai Ü, Soós K, Penke B. *Epitaxial assembly kinetics of mutant amyloid beta 25-35 fibrils.* From Solid State to Biophysics V. International Conference and Biophisics Summer School. Dubrovnik, Croatia, 2010.

Horváth A, Aradi M, Schwarcz A, Kövér F, Dóczi T*. A funkcionális MR (fMRI) szerepe a kómás betegek alapvető kognitív funkciójának vizsgálatában.* Student Research Conference, Pécs, 2010.

Horváth A, Aradi M, Perlaki G, Orsi G, Schwarcz A, Büki A, Kövér F, Dóczi T, Bogner P*. The evaluation of comatose brain with fMRI, DTI and spectroscopy.* V. Young European Scientist Meeting, Porto, Portugal 2010.

Horváth A, Murvai Ü, Karsai Á, Kellermayer M*. Aß25-35_N27C amiloid fibrillumok epitaxiális növekedési kinetikája.* Student Research Conference, Pécs, 2009.

Szili K, **Horváth A**, Kálmándy-Pap P. *Betegség? Nem butaság! Dyslexia vizsgálata különböző korosztályokban.* 15th Students' Scientific Conference, Targu Mures, Románia 2008.

Horváth A, Sétáló Gy., Szeberényi J. *A proteaszóma-gátlás hatásainak vizsgálata PC12 sejtek túlélésére.* South-Hungarian Regional Student Research Conference, Paks, 2006.

8.5 Supervised undergraduate theses

Herczeg Boglárka. *Kin segít a shunt? - Liquorvolumetria hydrocephalusos betegeknél.* University of Pécs, Medical School, 2016

Dege Dorina*. A gliómás gradus, molekuláris biológiai markerek és MR perfúziós paraméterek összefüggéseinek vizsgálata.* University of Pécs, Faculty of Health Sciences, 2016

Horváth Péter. *A teljes agy besugárzást követő agyi atrófia meghatározása MR volumetriával.* University of Pécs, Medical School, 2016

9. Acknowledgements

All the work presented in this thesis could not have been carried out without the help of many people, to whom I owe a great debt of gratitude.

First, I wish to thank my supervisor, Prof. Péter Bogner for teaching me the basics of neuroscience research, his continuous support, efforts, guidance and irreplaceable help in summarizing my thesis. I am most grateful to Dr. Mihály Aradi for introducing me as a student research fellow into the world of neuroimaging. I would like to thank Prof. Tamás Dóczi and Dr. Ferenc Kövér for the technical and professional support of my work.

I would like to also thank the members of the research group, Dr. Arnold Tóth, Dr. Gábor Perlaki, Dr. Gergely Orsi and Szilvia Anett Nagy for constantly advising and helping me through all these years regarding both the theoretical and technical parts of the research and for sharing their expertise with me. They answered a series of my questions every day tirelessly and patiently, providing their knowledge and insight in the field of MRI.

I would like to thank all my colleagues at the Diagnostic Center of Pécs and the University of Pécs, in particular, Viktória Tamás, Kristóf Biczó, Péter Bódi, Szilvia Waller and Zsuzsanna Baranyai.

Special thanks must be paid to my friends, Dr. Anna Cseh, Dr. Bálint Scheich, Judit Sámson and Dr. Anna Budai. Most special thanks to Dr. Csanád Várallyay for his continuous support.

I express my gratitude to my parents, my brother, my grandmother and other members of my family for their love and for supporting and encouraging me through all these years.